Everything you wanted to know about phase and reference frequency in one- and two-dimensional NMR spectroscopy

Sheberstov, Kirill; Sistare Guardiola, Eduard; Jeannerat, Damien

How to cite

SHEBERSTOV, Kirill, SISTARE GUARDIOLA, Eduard, JEANNERAT, Damien. Everything you wanted to know about phase and reference frequency in one- and two-dimensional NMR spectroscopy. In: Magnetic Resonance in Chemistry, 2020, vol. 58, n° 5, p. 376–389. doi: 10.1002/mrc.4938

This publication URL: https://archive-ouverte.unige.ch/unige:132660
Publication DOI: 10.1002/mrc.4938

Everything you wanted to know about phase and reference frequency in one- and two-dimensional NMR Spectroscopy

Kirill F. Sheberstov [a], Eduard Guardiola Sistare [b], Damien Jeannerat [b,*]

[a] Johannes Gutenberg-Universität, Mainz, 55099, Germany

[b] Department of Organic Chemistry, University of Geneva, Geneva, 1211, Switzerland.

Post-review manuscript published in
Magnetic Resonance in Chemistry

https://onlinelibrary.wiley.com/doi/abs/10.1002/mrc.4938

Abstract

The fundamental concept of phase is discussed in this tutorial aimed at providing students with an explanation of the delays and processing parameters they may find in NMR pulse programs. We consider the phase of radio-frequency pulses, receiver, magnetization and how all these parameters are related to phases and offsets of signals in spectra. The impact of the off-resonance effect on the phase of the magnetization is discussed before presenting an overview of how adjustment of the time reference of the free induction decay (FID) avoids first-order correction of the phase of spectra. The main objective of this tutorial is to show how the relative phase of a pulse and the receiver can be used to change the reference frequency along direct and indirect dimensions of NMR experiments. Unusual applications of phase incrementation with non-90 degree angles will be illustrated on 1D and 2D NMR spectra.

1 | Introduction

Phase appear at every turn in conversations about NMR spectroscopy and refer to many different features, often without clear distinction. This can make it quite mystifying to beginners. Even a simple 1D NMR spectrum involves a total of four phase-related quantities: the phase of the excitation pulse, the phase of the receiver, the phase of the detected magnetization, and finally the phase of the peak resulting from the phase correction of the spectrum.

This tutorial will carry readers through a journey addressing some interesting but overlooked aspects of basic pulsed NMR spectroscopy. It will discuss some mysterious delays and parameters having to do with phase that can be found in modern pulse programs that are not explained in pulse sequence manuals. We have in mind the short delay between the excitation pulse and the start of the acquisition in 1D experiment, the subtraction of a fraction of pulse duration from t_1 in some two-dimension experiments, the argument for using 180° as the first-order corrections in the indirect dimension of some 2D spectra, *etc*. We shall not attempt to provide a complete background of NMR spectroscopy - this can be found in standard textbooks[1-4] - but introduce them at the relevant point of a focused presentation of a simple excitation pulse (Section 2) followed by detection (Section 3). A comparison of direct and indirect detection will follow in Section 4.

One of the puzzling questions for beginners concerns the frequencies visualized in NMR spectra. On modern NMR spectrometers, the precession frequencies are usually in the order of hundreds of MHz, however, the maximal frequencies in NMR spectra are typically in the tenths of kHz. In order to explain this apparent inconsistency we should remind that the "carrier" frequency ν_{cf} is subtracted from the NMR signal. The frequencies observed in a spectrum are often called "offset" frequencies and are given by:

$$\Delta_0^i = \nu_0^i - \nu_{cf} \qquad (1)$$

where ν_0^i is the Larmor frequency of the signal i expressed in Hertz. This subtraction is performed for direct observation (of 1D and the t_2 axis of 2D experiments) using a quadrature detection[2, 3] we shall discuss in some details below. Concerning the indirect detection of two-dimensional experiments it is interesting to already point out that signals in t_1 directly appear as Δ_0^i, because the pulses, which flank the t_1 evolution, are phase-coherent (see below) and this acts as the subtractor of ν_{cf}. An important exception is *J*-spectroscopy where the Larmor precession is refocused at the end of t_1.

A loss of information about the relative signs of the frequencies of signals may occur because of the subtraction of the reference frequency (Eqn 1). The ability to distinguish these relative signs is called a "frequency discrimination". This is particularly important when the carrier is located in the middle of the NMR spectrum. In contrast, frequency discrimination is not necessary when the carrier frequency is set outside the range of observed frequencies (e.g. $\nu_{cf} < \{\nu_0^i\}$). We should see, in Section 2, a disadvantage of this circumvention and, in section 3.7 the elegant solution introduced by Redfield using a phase incrementation of the receiver resulting in a virtual shift of the carrier frequency. We will call this apparent carrier frequency, the reference frequency ν_{ref} which may differ from ν_{cf}. A clue towards the understanding of the relationship between phase and reference frequency appears

when realizing that a phase incrementation introduces a time dependence that can be characterized by a frequency.

This tutorial will demonstrate mathematically and graphically how the carrier frequency can be virtually shifted using the phase of the receiver during direct detection and how the 2D quadrature detection method called TPPI (Time Proportional Phase Incrementation)[5] operates. It will also show that the phase incrementation is not limited to 90° increment, thus providing a superior control over reference frequencies in one- and two-dimensional experiments.

2 | Hard pulses

NMR spectrometers are equipped with frequency synthesizers that permanently generate sinusoidal radiofrequency (RF) signals (dotted line in Figure 1). Hard pulses are produced by opening, for a few microseconds, an electronic gate between the synthesizer and the amplifier connected to the coil located in the probe head.

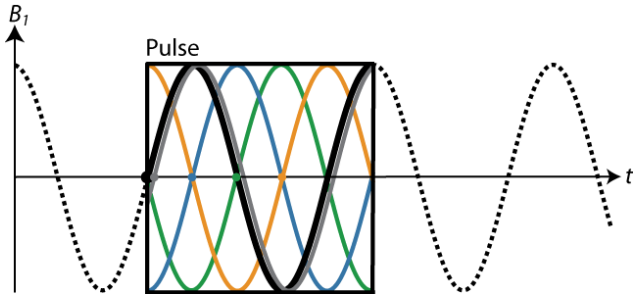

Figure 1 Radio-frequency pulses and their phases. The *x* pulse (broad black line) has a phase zero: it is aligned with the carrier frequency (dotted black line). The grey pulse is shifted by 20°. The pulses with phase 0° (black), 90° (blue), 180° (green) and 270° (orange) are called *x, y, -x*, and *-y* according to the direction of the corresponding vectors in the rotating frame.

The effect of these pulses will be to tilt the magnetization of the nucleus resonating at this frequency from the equilibrium state along the direction of the main magnetic field (*z*-axis) towards the *x*/*y* plane where its free precession will be recorded until its decay. The phase of the pulse therefore determines the phase of the detected signal.

The signal produced by the synthesizer is also used for referencing the detection of the signal. It is subtracted during the quadrature detection in a similar manner as pulses, it can be given any arbitrary phase shift, ϕ_{rec}, which is called the receiver phase. (see the Supplementary Material)

2.1 The phase of hard pulses

On modern spectrometers, the RF pulses can be given a phase which corresponds to the direction of the pulse in the rotating frame. This is obtained by shifting the RF signals (see colored signals in Figure 1 and the Supplementary Material) to obtain any desirable phase ϕ_p relative to the carrier. This produces a RF signal

$$B_1(t) = B_1 \cos\left(2\pi\, \nu_p t + \phi_p\right) \qquad (2)$$

where ν_p is the frequency of the pulse, B_1 is the amplitude of the RF field (see below), and ϕ_p is its phase. Note that the frequency of the pulse can also be shifted (see the Supplementary Material), but it is usually set to correspond to the frequency of the middle of the spectral range of the isotope of interest and $\nu_p = \nu_{cf}$.

Most of the time, the phase shift is a multiple of 90°, but some applications use other increments, in particular in multiple-quantum NMR spectroscopy.[6-9] Alternating the phases of pulses and detector in successive acquisition is a central tool of NMR spectroscopy called "phase cycling". It is used to cancel out unwanted signals by adding and subtracting FID's according to the phase of pulses and adding up the desired magnetization.[1-4]

The pulse amplitude B_1 in Eqn 2 corresponds to the strength of the applied RF magnetic field. It is set on the spectrometer in dB or in Watt depending on the spectrometer manufacturer. But in the NMR literature, it is of common practice to relate a magnetic field strength to a precession frequency expressed in Hz (or kHz). This has the advantage to directly express the nutation frequency, *i.e.* the frequency of the precession of the spin magnetization about the B_1 field:

$$\nu_{rf} = \left|\frac{1}{2}\frac{\gamma B_1}{2\pi}\right| \qquad (3)$$

where γ is the nuclear gyromagnetic ratio, and the factor $\frac{1}{2}$ arises from the rotating wave approximation.[3] We follow here the convention used in "Spin Dynamics"[3] where the nutation frequency is always positive regardless the sign of γ, so the nutation happens according to right-hand rule for both nuclear types. The phase of the rotating frame in this convention $\varphi_{rf} = \pi$ for nuclei with $\gamma > 0$, and $\varphi_{rf} = 0$ for $\gamma < 0$, which is assumed in the Bloch spheres of this paper.[10, 11]

The product of the duration of the pulse τ_p and the nutation frequency ν_{rf} determines how much the magnetization will turn about the RF field. It is called the "flip" angle.

$$\beta = 360° \, \tau_p \nu_{rf}. \qquad (4)$$

It is often set to 90°, but in most routine 1D NMR experiments, the desired tilt angle is not 90°, the angle resulting to the strongest signal of fully relaxed magnetization, but 30°. Compared to a 90° pulse, such a "small flip or tilt angle" produces half the signal (because sin(30°) = 0.5) which is detrimental. But the recovery delay can be reduced to an extent that more than compensates this reduction because the magnetization starts closer to the equilibrium position.[1] Note that the actual optimal angle, called the Ernst angle[12] requires the knowledge of the T_1 relaxation time, making it of little practical use.[1]

In general, a hard RF pulse with a flip angle β, and a duration τ_p should have an amplitude

$$B_1 = 4\pi \frac{\beta}{360°\gamma} \frac{1}{\tau_p}. \qquad (5)$$

2.2 Effects of the offset on the phase of the magnetization

A 90° pulse has a typical duration of 10 µs which, according to Eqn 4, corresponds to a 25 kHz nutation frequency. In the rotating frame (considering that it rotates with a frequency ν_{cf}), the on-resonance magnetization, (*i.e.* the magnetization of a spin resonating at the frequency of the $\vec{B}_1$ field) will follow a circular trajectory across the surface of a Bloch sphere about $\vec{B}_1$. At 25 kHz, it makes a quarter cycle towards the *x/y* plane in 10 µs (see Figure 2A).

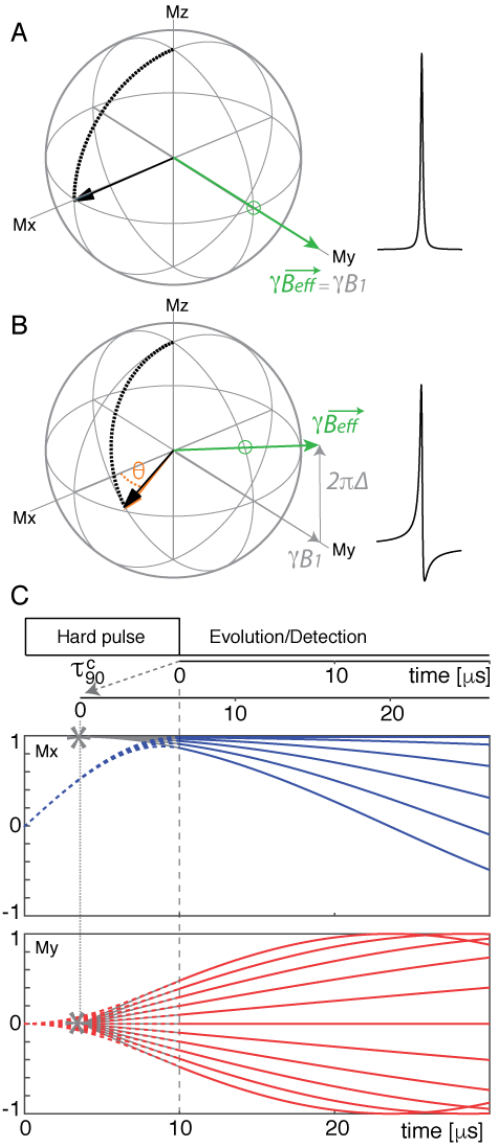

Figure 2 Bloch spheres representation of the trajectory of the on-resonance (A) and off-resonance (B) magnetization during a 90° RF pulse. The off-resonance trajectory was calculated for an offset frequency Δ = 12.5 kHz ($\nu_{rf}/2$). The phase shift θ was measured on the projection of the trajectory of the magnetization onto the *x/y* plane. (C) In-plane components of the magnetization during and after the pulse for Δ ranging from $-\nu_{rf}/2$ to $\nu_{rf}/2$ and steps of $\nu_{rf}/10$. The star indicates the virtual origin of the periodic function representing the free evolution of the magnetization starting at the end of the pulse.

When the spin is off-resonance, that is when its Larmor frequency differs from the carrier frequency by Δ, the effective field $\vec{B}_{eff}$ must be considered instead of $\vec{B}_1$ alone. The Figure 2B shows that the coordinates of $\gamma\vec{B}_{eff}$ are γB_1 and $2\pi\Delta$ in the *x* and *z* dimensions respectively and its norm

$$|\gamma \mathrm{B}_{\mathrm{eff}}| = \sqrt{\gamma \mathrm{B}_1^2 + (2\pi\Delta)^2}. \qquad (6)$$

In general, the magnetization follows a trajectory deviating from the *x/z*-plane and ends up slightly off the *x* direction (see Figure 2B). This causes the magnetization to display a phase shift θ corresponding to the angle between the *x*-axis and the projection of the magnetization onto the *x/y*-plane. This shift can be calculated by simple integration and turned out to be reasonably linear (see Figure S1 in the Supplementary Material) over the usual spectral window of ^{1}H and ^{13}C isotopes.

This phase deviation of the magnetization, in turn, causes a phase shift β in the spectrum. This will give some dispersive character to the peaks with the characteristic negative component (see the peaks on the right of Figure 2A and B and the Real component of the spectrum in Figure 3). A pure absorption shape can be restored using a first-order correction; the well-known process by which most spectra are tuned - often manually - to eliminate any negative contribution due to a dispersive component and present spectra with the pure-absorptive lineshape.[1-4] In the absence of signal overlap, the phase of signals can be measured in the DISPA representation of spectra (see left part of Figure 3).[13, 14]

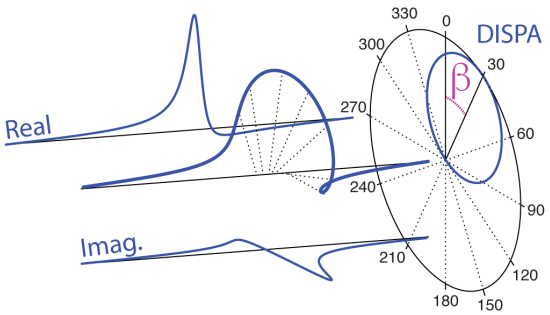

Figure 3 Three-dimensional representation of a simulated spectrum of a singlet with a 30° phase shift. It is composed of the real (horizontal project) and imaginary (vertical projection) components of the spectrum. Note that the projection of the spectrum along the frequency axis (Dispersion *versus* Absorption – or DISPA representation) of a pure Lorentzian shape corresponds to a circle (left). The angle between its top position and the vertical axis corresponds to the phase of the signal. In a well-phased spectrum, the curls should all point up.

2.3 Avoiding phase correction of the spectra by shifting the time reference of the FID

An elegant alternative to the first-order phase correction caused by chemical-shift evolution during hard pulses consists in moving the time reference of the acquisition in such a manner as to cancel the linear component of the phase shift. Indeed, the magnetization evolves during the pulse as shows the dashed colored lines in Figure 2C. As a consequence, the start of the acquisition of the FID does not correspond to the true beginning of the in-plane evolution. Interpolating the trajectory of the

transverse magnetization back from the end of the pulse shows that there is a point where they all join (see the stars in Figure 2C).

Setting the time reference of the detected signal to $-t^c_{90°}$ before Fourier Transformation eliminates the need to apply a first-order correction. For a 90° pulse,

$$t^c_{90°} = \frac{2}{\pi}\tau_p. \quad (7)$$

This property is exploited on modern spectrometer using digital filters to define the reference time (on Bruker instruments this time is called *acqt0*) of the acquisition of the FID and to eliminate most of the first-order phase shift introduced by hard pulses.

For a pulse with $\beta < 90°$, the correction is smaller because the phase dispersion is less active when the magnetization is far from the transverse plane. In general, the time correction is

$$t^c_\beta = \frac{\beta}{90}\frac{2}{\pi}\tau_p, \quad (8)$$

when $\beta < 90°$. In the absence of digital filtering, a manually set first-order correction (*phc1* in the Bruker language) would therefore be set to:

$$-360 \cdot 2 \cdot SB \cdot t^c \quad (9)$$

where *SB* is the sampling bandwidth (sometimes called "spectral width" – SW in the Bruker language) of the spectrum in Hz. This angle, expressed in degrees, corresponds to the difference in the phase of the two ends of the spectrum.

2.4 Off-resonance effect, out-of-phase magnetization and excitation profile

In order to observe the bandwidth limitation of hard pulses, one should study the effect of the pulse beyond the $\pm$ 0.5 ν_{rf} boundaries. The dotted lines in Figure 4A and 4B plot the trajectories of the magnetization for values of $1\nu_{rf}$ and from 2 to $6\nu_{rf}$, respectively. The position of the magnetization at the end of the pulse, *i.e.* the moment when the free evolution starts, is highlighted with a blue line in Figure 4A and 4B. The projection of these positions on the *x/y* plane (bold black line) represents the amplitude and phase of the signal that can be directly detected during the free evolution. The *Mx* and *My* components and the norm of these vectors plotted as a function of the frequency offset constitute the so-called “excitation profile” of the pulse shown in Figure 4D.

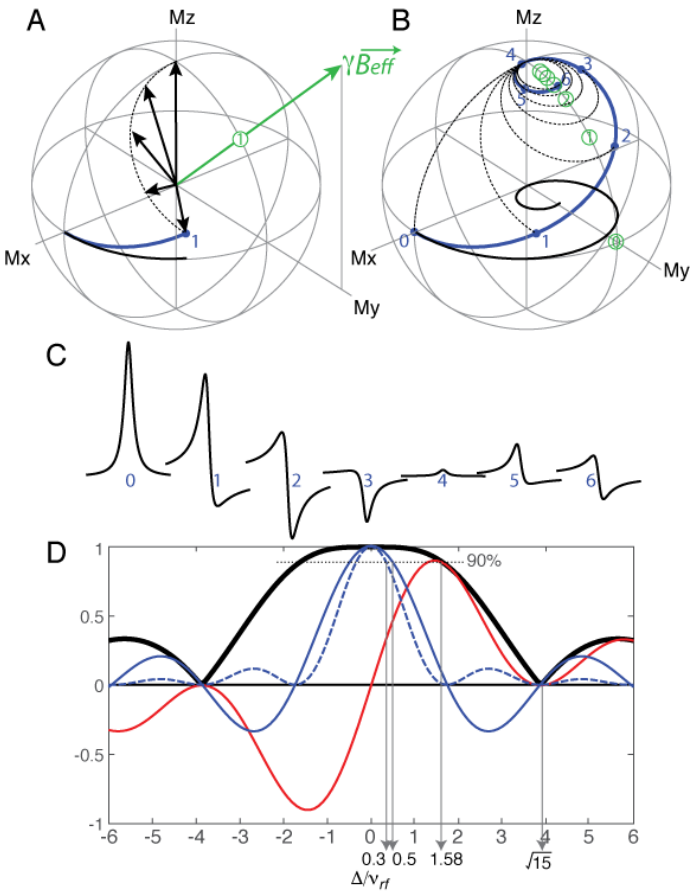

Figure 4 (A, B) Bloch spheres of the magnetization following a 90° pulse. The full trajectories of the magnetizations were plotted using dashed lines for $\Delta/\nu_{rf} = 1$ (A) and for integer values ranging from 1 to 6 (B). Open green circles indicate where the effective-field vectors penetrate the surface of the sphere, *i.e.* the direction about which the magnetization (dotted line) precesses. (C) Out-of-phase singlets with phase shift of 0, 55.0, 101.8, 143.7, 5.2, 48.8, 93.7° respectively. (D) Excitation profile of the final position of the magnetization following the pulse as a function of Δ/ν_{rf}. The bold black line corresponds to the norm of the vector formed of the *Mx* (blue line) and *My* (red line) components of the magnetization. The dashed blue line corresponds to the square of the *Mx* component, the expected profile of a combination of two consecutive pulses.

For an offset of $1\nu_{rf}$, the magnetization ends up with nearly equal *Mx* and *My* components, but the signal amplitude is expected to be almost quantitative as the projection is quite close to the *x*/*y*-unit circle (Figure 4A) *i.e.* high on the excitation profile (bold line in Figure 4D). The signal amplitude is quite satisfactory, but a phase shift of about 45° will be observed. For $2\nu_{rf}$, the magnetization draws almost a quarter-circle, ending up quite high above the *y* axis and with a small *Mx* component of opposite sign relative to on-resonance magnetization. (see Figure 4B) In this case, that is at frequencies $\pm 2\nu_{rf}$, the $-y$ pulse is not producing *Mx*-magnetization (as on resonance), but *My*-magnetization. Whether a phase shift is problematic or not depends on what follows the pulse and is discussed in the next two paragraphs.

When the magnetization is detected after the pulse - as in a simple 1D pulse-detection experiment - the signal intensity is proportional to $\sqrt{{M_x}^2 + {M_y}^2}$ (continuous

line in Figure 4D). In this case, the boundaries of the 90% efficiency (horizontal dashed line in Figure 4D) is found at $\pm 1.58 \cdot \nu_{rf}$ which corresponds to a range of $\pm$39.5 kHz for a 10 µs excitation pulse. But, one should remember that a signal at these boundary positions will be nearly 90° out of phase (see the position 2, in Figure 4B).

When the magnetization is not detected immediately after the pulse, but further transformed by hard pulses (for example in 2D experiments, when using *z*-filters, [15] spin echo, *etc.*), only one component of the magnetization can be exploited : the *x* component which has a 90% efficiency covering only $\pm 0.5 \cdot \nu_{rf}$. This corresponds to roughly one third of the bandwidth of the direct detection. In many cases, and because of the combined imperfections of the two pulses, the ideal profile corresponds to the square of the *Mx*-profile and the 90% is further reduced to $\pm 0.3 \cdot \nu_{rf}$. In practice it may be even smaller because of inhomogeneity in the B_1 field caused by the imperfections of the RF coil.

The offset corresponding to the first minimum of the excitation profile is found at

$$\Delta = \frac{\sqrt{(360/90)^2 - 1}}{\tau_p/_4} = \frac{\sqrt{15}}{\tau_p/_4} = \sqrt{15}\nu_{rf}, \qquad (10)$$

and corresponds to a magnetization drawing a full circle ending-up along the *z*-axis. (See "4" in Figure 4B) This minimum can be understood by the fact that the corresponding spins have felt an effective field during the second half of the pulse exactly cancelling the one of the first half of the pulse.

2.5 Further reading

The hard pulses are still quite commonly used even if numerous alternatives have been introduced. Their discussion is beyond the scope of this article but we shall mention of few of them. The hard pulse can be improved, for example, by replacing the 90 with a 270 degree rotation[16] to make them self-refocusing pulses (see the Supplementary Material to compare the trajectories of 270° and 90° pulses). The off-resonance effects of hard pulses can also be reduced using composite pulses[17-21] consisting of catenated multiple pulses - typically three - with different phases. But they can also be replaced by pulses that vary either in amplitude (shaped pulse) [22, 23] or frequency (e.g. CHIRP pulses).[24-26]

Another interesting property of the off-resonance effects were studied by D. Suter *et al.*[27], who showed how a non-linear phase evolution of the magnetization is related to geometrical phase factors, *i.e.* the phase acquired due to motion of spins along different trajectories. The reader can refer to the numerous reviews available on these topics knowing that the above-mentioned references were selected arbitrarily.

3 | Quadrature detection

3.1 "Complex" detection of the free-induction decay

After an excitation pulse, the magnetization evolves in the *x*/*y* plane and generates the detected signal. This magnetization is decomposed into $D_x = cos(2\pi\Delta_0 t)$ and $D_y = sin(2\pi\Delta_0 t)$ components using quadrature detectors (see the Supplementary Material). The use of "complex numbers" allows one to use Euler

formula to combine D_x and D_y values as the real and imaginary components of a complex function

$$D_+ = D_x + iD_y = cos(2\pi\Delta_0 t) + isin(2\pi\Delta_0 t) = e^{i2\pi\Delta_0 t} \qquad (11)$$

where $i = \sqrt{-1}$. Note that relaxation is not considered here, but would simply introduce an $exp(-t/T_2)$ factor to account for the signal decay.

The cos and sin components of a positive signal with a 2 Hz offset frequency are plotted in Figure 5A and 5B respectively together with their three-dimensional representation (in blue).

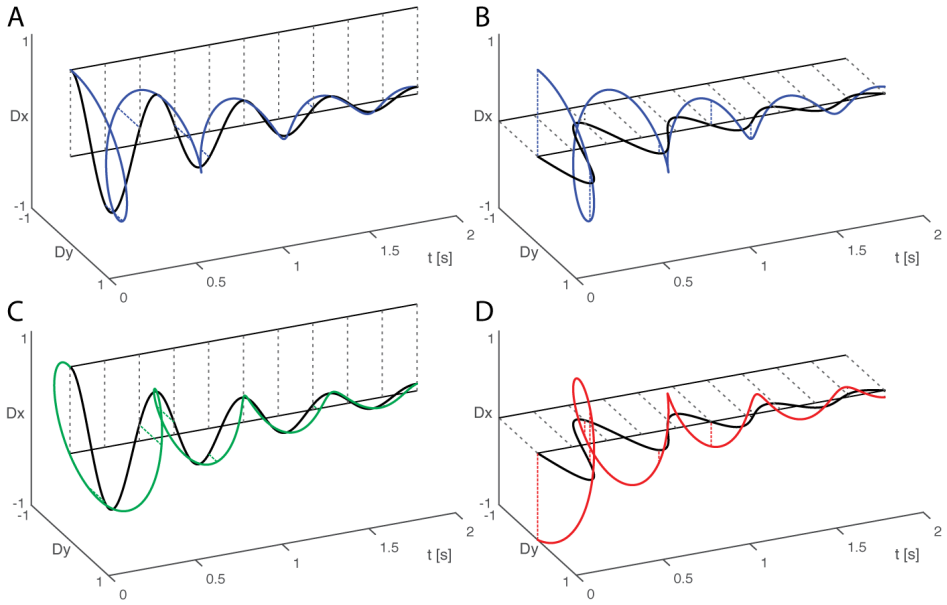

Figure 5 Three-dimensional representation with projection of the D_x (A) and D_y (B) components of a signal with an offset frequency of $\Delta_0 = +2$ Hz (blue). (C, D) Positive (green) and negative (red) signals with $\Delta_0 = -2$ Hz frequencies. For clarity the Mx- and My-components are projected vertically and horizontally respectively (black lines). The relaxation time $T_2 = 5/\pi$ s for this and the following figures.

3.2 "Standard" quadrature

The "classical" detection of NMR signals uses two outputs in order to measure the orthogonal components simultaneously. The principle of quadrature detection is described in the Supplementary Material. In short, the carrier frequency of the pulses is set to the middle of the spectral range of the isotope so that the excitation profile is centered and the off-resonance effects are minimized (see Figure 4). When the two outputs of the quadrature detector are perfectly orthogonal and assuming the magnetization lies along the *x*-direction in the rotating frame after the pulse, the signal induced in the receiver are the real (D_x) and imaginary (D_y) components of D_+ (see *Sim* detection in Table 1). A simulated spectrum acquired using this quadrature is shown at the top of Figure 6.

Table 1. Phase sequences and detection times used for frequency discrimination.

										Sign of aliased signals[2]				
									Nyquist[1]	with initial t_1 evolution =				
n[3] =	0	1	2	3	4	5	6	7	violation	0	inc/2	inc	Artifacts[4]	Remark
Real	x	x	x	x	x	x	x	x	folding	+	−	+		CF-shift[5]
Real[6]	x		x		x		x		aliasing	+	−	+	middle	FT-shift[7]
Imag.	y		y		y		y							
Real[8]	x	y	x	y	x	y	x	y	folding	−	+	−	middle	
Real[9]	x	y	-x	-y	x	y	-x	-y	folding	−	+	−	bottom only	
Real[10]	x		y		-x		-y		aliasing	+	−	+	top and bot.	
Imag	y		-x		-y		x							

[1] See Section 4.1.

[2] See Section 4.3.

[3] At time $t = n\ dw$, where dw is the dwell time of the sampling. The phases x, y, $-x$ and $-y$ correspond to 0, 90, 180 and 270° respectively.

[4] According to Ref.[28]

[5] The carrier frequency has to be set to the side of the spectrum for frequency discrimination.

[6] Called Sim and States for direct and indirect detection in the Bruker language.

[7] The two halves of the spectrum have to be swapped after FFT to correct the scale.

[8] Called Seq and QSEQ for direct and indirect detection in the Bruker language. The relative phases of the pulses for QSEQ and TPPI are identical. For QSEQ, the relative phases are [x, y, x, y] and the detector alternates as [$x, x, -x, -x$] while for TPPI, the cycle is [$x, y, -x, -y$] for the pulses and the detector phase is constant on x.

[7] Called TPPI for indirect detection in the Bruker language.

[8] Called States-TPPI for indirect detection in the Bruker language. Same properties as for E/AE.

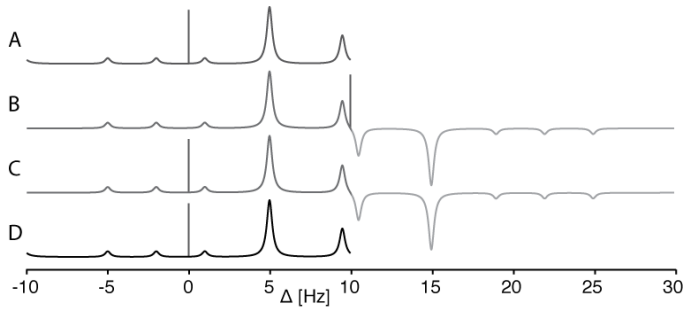

Figure 6 Simulated spectra obtained after Fourier transformation of the FID acquired using (A) a simultaneous detection of the two channels of the quadrature detector, (B) a single-channel detection with the ν_{cf} at one side of the spectrum, (C) the single-channel detection with 90° phase incrementation (Redfield trick) and (D) the simultaneously detection of orthogonal components and phase incrementation. The phase of the detector was aligned to the excitation pulse. When the detector is set to 45 or 90 degrees out of phase relative to the excitation pulse, the negative peaks appear dispersive or positive respectively (see Figures S4 in the Supporting information). Note that one half of the data generated by the Fourier transform is discarded when single-channel detection is used.

3.3 Fourier transformation

The NMR spectra are usually obtained using the Fourier transform (FT), which converts the time-domain signal into a frequency domain spectrum: [1-4]

$$S(\upsilon)= \int_{-\infty}^{\infty} D(t)e^{-i2\pi\upsilon t}dt. \quad (12)$$

When combining Eqns 11 and 12 the integral becomes

$$S(\upsilon)=\int_{-\infty}^{\infty} e^{i2\pi\Delta_0 t}e^{-i2\pi\upsilon t}dt = \int_{-\infty}^{\infty} e^{i2\pi(\Delta_0-\upsilon)t}dt, \quad (13)$$

Such a spectrum consists of a single delta function $\delta(\Delta_0)$, a function that returns zero except when $\upsilon = \Delta_0$. In other words, a signal can be observed at the frequency Δ_0. Including the exponential decay would produce absorptive and dispersive Lorentzian lineshape centered at Δ_0 in the real and imaginary components of the spectrum respectively.

When considering discretely recorded data, the range of correctly determined frequencies depends on the dwell time - the time between two sampled data points - according to the Nyquist condition, which is usually expressed as[1-4]

$$dw = 1/2SB. \quad (14)$$

In the case of standard acquisition data ("Sim" in the Bruker language), the sign discrimination being possible, the effective frequency range is [–*SB*/2 : +*SB*/2].

3.4 Alignment of the pulses and receiver phases

The phase of the pulse and the receiver, φ_{p} and φ_{rec}, acquire some discrepancy because of the sensitivity of the resonant circuit to the experimental conditions in the vicinity of the detector's coil. This phase difference φ_{diff} on the detected signals influences the detected signal:

$$\mathrm{D}_{+err} = e^{i[2\pi(\Delta_0-\upsilon)t+\varphi_{diff}]}. \quad (15)$$

A spectrum with φ_{diff} = 30° is shown in Figure 3. A property of the exponential function allows to isolate the φ_{diff} term as

$$\mathrm{D}_{+diff} = e^{i2\pi(\Delta_0-\upsilon)t}e^{i\varphi_{diff}}. \quad (16)$$

The zero-order phase corrections consist in multiplying the signal D_{+diff} with a phase correction functions $e^{i\varphi_{corr}}$ to obtain the corrected signal:

$$\mathrm{D}_{+} = e^{i2\pi(\Delta_0-\upsilon)t}e^{i\varphi_{diff}}e^{i\varphi_{corr}}. \quad (17)$$

The zero-order correction φ_{corr} is adjusted manually or automatically until the spectrum shows an absorption lineshape. This occurs when $\varphi_{\mathrm{corr}} = -\varphi_{\mathrm{err}}$, which cancels the $e^{i\varphi_{diff}}$ term because

$$e^{i\varphi}e^{(-i\varphi)} = 1. \quad (18)$$

When considering the 3D representation of the signal (see Figure 5), the phase difference has the effect of turning the whole spiral by a φ_{diff} angle. This rotation is simply corrected by a rotation in the opposite direction.

Note that the zero-order phase difference can be corrected in the time or the frequency domains. But the correction of frequency-dependent phase is done using a first-order correction in the frequency domain. First-order correction in the time domain has a completely different effect: it shifts the frequencies of signals as will be shown in Section 3.7. Finally, note that the first-order phase correction in the frequency domain is mathematically not a perfect solution to restore a pure absorption lineshape, especially in case of severe overlap and the presence of a dispersive component[3]. It may, for instance, cause a "rolling" of the baseline requiring further processing.

3.5 The problem with single output hardware

Historically, signals have not always been detected using quadrature detection. Early spectrometers could detect only one component of FIDs. The problem with single-output detection (only D_x or D_y) is that the relative signs of the signals cannot be determined unambiguously after subtraction of the carrier frequency. For the *x* component, the problem is an ambiguity in the sign of the frequency because $cos(\Delta) = cos(-\Delta)$. This can also be understood by observing that those projections of positive and negative frequencies have the same shape (compare the projections in Figure 5A with Figure 5C). For the *y* channel, the problem is that positive signal cannot be distinguished from negative signals with the opposite frequency because $\sin(\Delta) = -\sin(-\Delta)$ (compare Figure 5B with Figure 5D).

The application of the FT to *real* data (called *real* because they miss the orthogonal *imaginary* component to make them *complex*) results to two delta functions, instead of one. When considering the *cos* component, a property of the trigonometric functions expressing the $\cos(a)$ as $(e^{ia} + e^{-ia})/2$, the result of the Fourier transform is

$$S(2\pi\nu) = \int_{-\infty}^{\infty} \cos(2\pi\Delta_0 t)e^{-i2\pi\upsilon t}dt = \int_{-\infty}^{\infty} \frac{e^{-i2\pi(\upsilon-\Delta_0)t} + e^{-i2\pi(\upsilon+\Delta_0)t}}{2}dt. \quad (19)$$

This corresponds to two non-zero elements for $+\delta(-\Delta_0)$ and $+\delta(\Delta_0)$ often characterized as "inphase" or $[+\,+]$ pattern. For the *sin* component, $\sin(a)$ expressed as $(e^{ia} - e^{-ia})/2i$, the FT results to

$$S(2\pi\nu) = \int_{-\infty}^{\infty} \sin(2\pi\Delta_0 t)\, e^{-i2\pi\upsilon t}dt = -i\int_{-\infty}^{\infty} \frac{e^{-i2\pi(\upsilon-\Delta_0)t} - e^{-i2\pi(\upsilon+\Delta_0)t}}{2}dt \quad (20)$$

which is corresponding to $-\delta(-\Delta_0)$ and $+\delta(\Delta_0)$ often called "antiphase" or $[-\,+]$ pattern.

Obviously combining the two components (Eqns 19 and 20) results to Eqn 13 with unambiguous frequency discrimination because the resulting spectrum is the sum of the $[+\,+]$ and the $[-\,+]$ patterns where one of the two lines cancels out to produce a single peak $[0\,+]$. Note that historically, the detection of the two components of the signal was relying on two separate electronic devices making the subtraction

imperfect. This was resulting in small so-called "quadrature images" at the $-\Delta_0$ frequency which can be seen as the results of the imperfect subtraction of signals with opposite signs. During the last 20 years, the digital quadrature detection systems deployed on NMR spectrometer avoid this problem.[29]

3.6 Avoiding single-channel problems with shift of the frequency to a spectral boundary

In order to avoid the problem with the sign of the peaks and the sign of their frequencies mentioned earlier, one solution consisted in moving the frequency of the carrier (affecting the RF pulses and the dectector) to one of the sides of the spectrum instead of the center.[12] The spectral window was set to double the effective value causing the dwell time to become twice as small. But instead of detecting *n* real and *n* imaginary points (each measured simultaneously), *2n* real data points were (sequentially) detected over the same acquisition time (see Table 1). The spectra obtained after Fourier transformation were twice as large (Figure 6B) but presented symmetry properties with respect their centers. Only one half of the produced data were stored as spectrum. The second half was discarded, being either symmetrical (with pure *cos* modulation), antisymmetric (with pure *sin* modulation) or more generally out-of-phase (when the cos and sin components were mixed). (See Figure S4 in the Supplementary Material). Note that this method has the disadvantage to introduce spectral discontinuity because signals that are accidentally cut at the spectral boundaries are not continuing at the other side, unlike those acquired using the simulteneous method (compare Figure 6A and 6C).

When using single-channel detection, the frequency range is [0 : SB] instead of [−SB/2 : SB /2] for the standard detection. In other words, the problem of negative frequencies is avoided by shifting the carrier frequency. The number of digitized points is the same (*2N* real instead of *N* complex data points) and the maximal evolution time is also the same. But a major drawback of this approach is that the pulses are not applied in the middle of the spectrum thus not optimal with respect to the offset effects discussed in Section 2.4.

3.7 Phase incrementation for quadrature detection

The solution to the problem of shifting the carrier frequency to a side of the spectrum was introduced in 1975[30] by Redfield and coworkers. It is quite interesting historically and also fundamental for understanding the TPPI quadrature schemes used in many multidimensional NMR spectroscopy.

The "Redfield trick" consists of avoiding the problem of negative frequencies by adding a virtual rotation of the detector with a frequency $\upsilon_{Red} = \mathrm{SB}/2$. This translates the range of detected frequencies to [−SB /2 : SB /2] instead of [0 : SB] and allows frequency discrimination with a single output detection. Instead of detecting signals with a constant phase, ($\varphi_{rec} = 0$) as in Figure 7A, the phase is incremented by an angle ψ for each detected point :

$$\varphi_{rec}(n) = n\psi, \qquad (21)$$

where *n* is the point number. For $\psi = 90°$, this phase series corresponds to 0, 90, 180, 270, 360, *etc*. which corresponds to the x, y, -x, -y, x, *etc*. directions in the rotating frame.

A mathematical demonstration of the relationship between the phase incrementation and the frequency shift is given in the Supporting material while the 3D representations of Figure 7 demonstrates graphically how the 90 ° phase incrementation corresponds to adding SB /2 to the apparent frequency of signals.

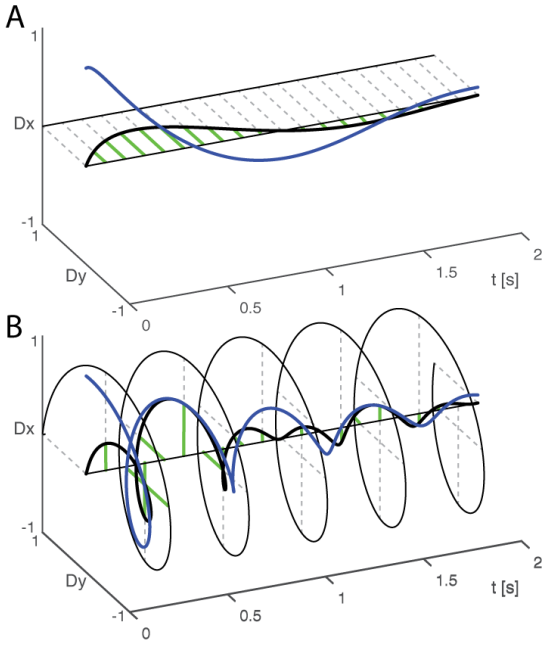

Figure 7 (A) Single channel detection of a decaying signal with an apparent frequency of 0.5 Hz (one cycle over 2 s). The 3D and projection on the *y* axis are plotted in blue and black respectively. Winding the time axis clockwise with a 90° increment at each point in a manner similar to the opening of a hand fan illustrates Redfield's sampling (B). The direction of the detector (grey dashed lines) is constant in A, but follow the outer black helix in B. The green ticks representing the signal amplitudes measured at discrete time intervals have the same length in A and B, but in B, the apparent frequency of the signal is decreased by 2.5 Hz (SB /2) and appear to be of –2 Hz (the bold blue line in B makes four turns over two seconds). The spectral width SB = 5 Hz is determined from the dwell time of 0.1 s using the Nyquist condition (Eqn 14). Note that the *y* axis was inverted relative to Figure 5 for clarity.

3.8 Setting the reference frequency to any arbitrary position

The phase incrementation does not necessarily move the apparent carrier to a side of the spectrum. It can be shifted to any desired frequency by setting the ψ angle to values other than 90°. The Figure 8 shows the effect of a 4.5° ($\pi/40$) incrementation in the case of a 5 Hz spectrum. The spectrum is shifted by 5/40 = 0.125 Hz which is expected knowing that a 90° ($\pi/2$) phase shift would causes a shift of signal of 2.5 Hz (SB /2) .

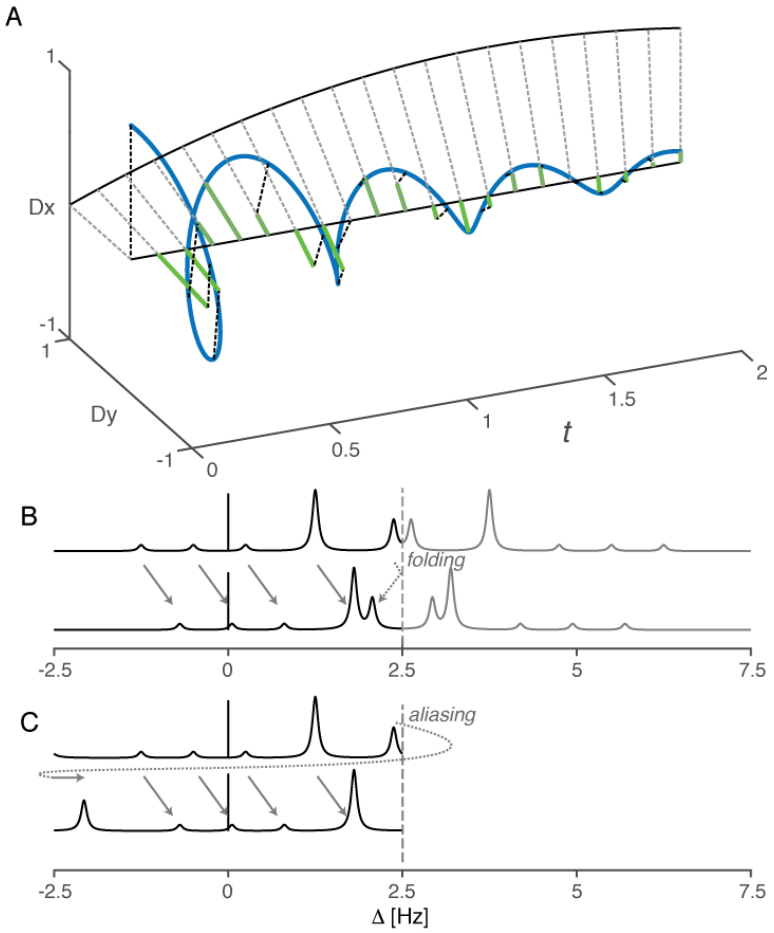

Figure 8 (A) Detection of a signal with a 4.5° phase incrementation. (B) Spectra obtained using Redfield and (C) complex quadrature detection. Compared to non-incremented detection (upper traces in B and C), the resulting spectra (lower traces in B and C) are shifted by 0.125 Hz.

Note that depending on the type of quadrature, the signals reaching the spectral boundaries are either folded in (Figure 8B) or aliased (Figure 8C). Spectral aliasing is usually preferred because it allows restoration of a normal spectrum by simple rotation (cycling permutation) of the data points relative to the scale.

4 | Two-dimensional NMR spectroscopy

4.1 Quadrature in the indirect dimension

Two-dimensional NMR spectroscopy requires two independent time evolutions to achieve frequency discrimination. In general, one needs to acquire sine and cosine modulated 2D datasets along the indirect dimension, although it is not always possible. The possibility to do this depends on the spin dynamics; for correlation spectroscopy it is achieved by changing the phases of some pulses flanking the t_1 evolution.

In the indirection dimension of correlation spectroscopy experiments, the detector is replaced by the pulse marking the end of the t_1 evolution. It is a hard 90° pulse, characterized by a frequency and a phase, the same two relevant properties of the detector in direct detection. Let us consider the situation of *phase cohorence,* occuring when the last pulse has the same frequency ν_{cf} as the first one and is produced by the

same synthesizer. What truly matters is the *relative* phase of the pulses of the indirectly detected isotope. Repeating the experiment twice by shifting the relative phase by 90° produces two orthogonal modulations for the indirect dimension. Note that it is important to properly digitize this data as hypercomplex numbers[31], thus giving independent control of the phases in the two spectral dimensions.[5, 32, 33]

Beside this important difference, the other aspects of quadrature are quite similar in direct and indirect detections, but some are named differently (see Table 1). In the indirect dimension, there is no problem of phase alignment between pulses and the detector, meaning that there is, in principle, no need of zero-order phase correction.

The right part of Table 1 reports some properties of diverse F1-quadrature[33]. The "standard" simultaneous detection is usually called "States" [32] or "SHR" (the initials of the authors of the paper States, Haberkorn, and Ruben) for indirect quadrature. The Redfield method applied to indirect dimensions is called QSEQ in the Bruker vocabulary, but a variant called TPPI (Time-Proportional Phase Incrementation)[5] is usually preferred. The States-TPPI, which combines the phase incrementation and simultaneous detection is favored when using spectral aliasing to improve the indirect F1 resolution[34]. Another advantage of States-TPPI and TPPI methods over States (Sim) is to avoid the zero-frequency artifacts to appear in the middle of the F1 dimension.

When the Nyquist condition is violated, signals outside the boundaries either appear as if the spectrum had been folded at the edges (folding) or at the other side of the spectrum (aliasing).[1]

4.2 Avoiding phase correction in the indirect dimension

An advantage of indirect detection is to facilitate the manipulation of the magnetization - something which is difficult to do when a data point is recorded every few microseconds. One can include, for example, a *J*-coupling refocusing pulse, such as the 180° pulse on the ^{1}H channel during the ^{13}C evolution of HSQC experiments. In some cases, one can also include a refocusing pulse to compensate for the chemical shift evolution during the pulses and the minimal inter-pulse delay (usually 3 us).

In most homonuclear experiments, such as COSY, TOCSY, *etc*., it is impossible to avoid a minimal t_1 chemical shift evolution because chemical shift refocusing is not possible. This minimal evolution may be quite short (a few microseconds corresponding to the minimal inter-pulse delay or the time of evolution during the pulses delimiting the t_1 evolution) or much longer (hundreds of microseconds) if a pulse-field gradient is included during the t_1 evolution time. In the second case, phasing the F1 dimension would be quite difficult and the spectra would probably need to be displayed in the magnitude mode. (The standard quick gCOSY[35, 36] experiments are of this type.) In the first case, a phase correction could be applied in F1 in a manner similar to the one presented in section 2.3, but the next paragraph will show that a property of the Fourier transform allows to produce spectra in pure absorption even when the spectra include aliased or folded signals.

4.3 Starting t_1 evolution with half the dwell time

The solution to the problem of evolution during the first t_1 increment is reminiscent of the one presented in paragraph 2.3. But instead of allowing the phase correction to take the value dictated by the t_β^c evolution time, one inserts an additional delay to the first t_1 evolution time so that $t_1^{init.} = \frac{1}{2} dw$.[37] According to Eqn 9, the

required phase correction will be exactly -180° (*phc1* on Bruker's software) because the phase of peaks will vary from 90 to -90 across the spectrum. The advantage of using this additional delay is that after phase correction, all signals, including the aliased ones, will appear in pure absorption. A pictorial demonstration is given as Supplementary Material, (Figure S5B), but the argument is that the phase correction needed at any F1 position is the same except for a $n \cdot 180°$ ($n \in \mathbb{N}$) residual phase which only influences the sign of the peak.

When the aliasing order n of a peak is odd,[34] which occurs for frequencies just outside the spectral boundaries, the sign of the peak will be opposite (see column "inc/2" in Table 1) relative the same aliased/folded peak in a spectrum recorded with an initial t_1 evolution equal to *zero*.

Note that using $t_1^{init.} = dw$ instead of $\frac{1}{2}dw$ avoids the sign alternation of aliased/folded signal (see figure S5C and column "inc" in Table 1).

4.4 Reference frequency in 2D NMR spectroscopy

We shall demonstrate in this section that a full control of the reference frequency in the indirect dimension of 2D experiments can be obtained by adjusting the phases of pulses in a similar manner as for direct detection. Before this, we will see that a simple change in the carrier frequency during t_1 is not always satisfactory.

The simplest method to shift spectra in the indirect dimension consists of changing the carrier frequency during the t_1 evolution time. Let's, for convenience, consider a simple two-pulse COSY sequence. Moving the carrier frequency just after the first pulse and setting it back to the middle of the spectrum just before the second pulse (see Figure 9) does the trick: The pulses are applied in the middle of the spectral window which is desired to limit off-resonance effects, and indeed the spectra will be shifted (only) in the indirect dimension after the usual double Fourier transformation. The main argument against this approach is technical. If modern spectrometers can easily switch frequency, this requires a short period of time, meaning that additional delays are introduced in the pulse programs. Even if we discussed solutions to this situation in the previous section, it is preferable to avoid them when possible. By contrast, the phase-adjustment approach only requires the ability of pulses to have user-definable phase, a feature which is included on modern spectrometers and requires no additional delay.

It may be counter-intuitive that changing a frequency during a period with no pulse can make any difference in the spectra. But, indeed, the number of cycles per time unit changes during the delay and the relative position in the cycle (the phase) will be different when the frequency is set back. The relative phase of the pulses is therefore affected as the Figure 9 illustrates.

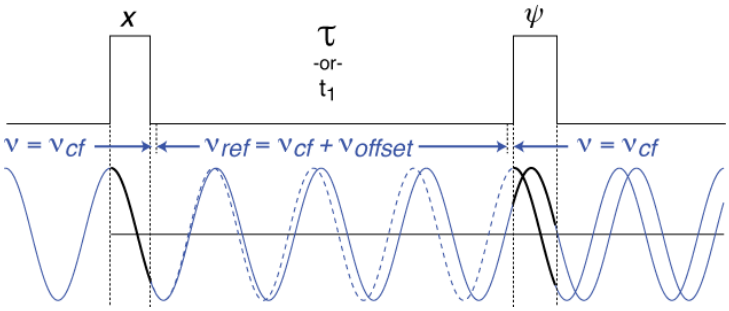

Figure 9 (a) Schematic illustration of the change of pulse phase (broad black lines) when the carrier frequency is shifted during the inter-pulse delay. The carrier frequency (blue) was increased (dashed line) during the inter-pulse delay. The same pulse can be obtained with no change of frequency by adjusting its phase according to the inter-pulse delay and frequency offset. For clarity of the figure, the frequencies and pulse durations were not drawn to scale.

Two *x*-pulses separated by some delay do not have the same relative phases if the carrier frequency changes during the delay. This demonstrates that adjusting the phases of the pulses is all that is needed to change the reference frequency in a two-dimensional spectrum.

A shift of the reference frequency can be obtained, without changing the actual RF frequency, by adding to the phase of one of the relevant pulses, the angle expressed in degrees

$$\psi = 360(\nu_{ref} - \nu_{cf})\tau, \qquad (22)$$

where τ is the difference between the time of application of the pulses, and ν_{cf} the carrier frequency. When the t_1 evolution period includes multiple pulses, such as in standard HSQC where a refocusing pulse is used, the phases of all the pulses of the indirectly detected isotope need to be adjusted relative to a reference. (See Supplementary material for the implementation on Bruker spectrometers.)

An example of application of a frequency offset by phase adjustment (FOPA) is shown in Figure 10 for an HSQC experiment acquired using the Echo/Antiecho quadrature scheme. Because signals outside the window are aliased with this quadrature scheme (see Table 1), a 30 ppm shift of the carrier frequency moves the spectrum down and brings the bottom part up (Figure 10B). The Supplementary Material presents how to control phases on Bruker spectrometer and shows the result of an implementation to the pulse programs of HSQC and DQF-COSY sequences.

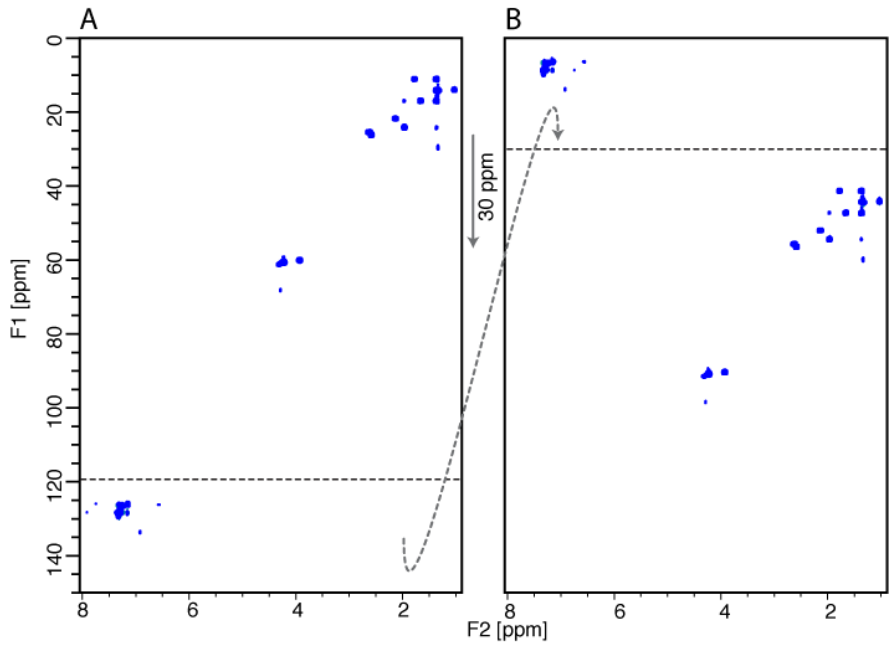

Figure 10. Comparison of a normal HSQC centered at 75 ppm (A) and an HSQC with a reference frequency shifted to 45 ppm by phase adjustment of the ^{13}C pulses during t_1 (B). The spectra recorded with E/AE quadrature (as here) have the same properties as the ones obtained with a States-TPPI quadrature. Aliased and non-aliased peaks have the same sign (see column t_1 evolution = 0 in Table 1).

When using the FOPA method, one should select quadrature causing aliasing (*versus* folding) because the resulting spectra are simply rolled/up as a whole (see Figure 10) instead of being folded which may cause offset-dependent overlap in F1 (not shown).

The non-90° phase incrementations (FOPA) was developed for a double-chemical shift encoding experiments[38] where the precise but ambiguous chemical shift information is encoded by the position of signals in the aliased spectrum while the complementary low-precision but unambiguous chemical shift is provided by their splitting[38, 39]. In these experiments, requiring a frequency shift to control the splitting of the signals, the delays associated to a double change of the carrier frequency position had to be avoided. These applications will be presented elsewhere.

5 | Conclusion

In the course of this tutorial, we laid out the relation between the phase and frequency of pulse and detector, and the phase of the signals in NMR spectra. We also delineated how phase incrementation can change the apparent frequency of signals. After discussing simple one-dimension pulse/acquisition experiments, we extended the scope of the presentation to the indirect dimension of two-dimensional experiments.

Finally, we showed how non-standard phase incrementation can produce any arbitrary spectral rotation when using complex data.

Experimental details

Most figures were generated using the Matlab/Octave programs available as Supplementary Material.

The spectra, including the one shown in the Figures in the Supplementary Material were recorded on a 300 MHz ^{1}H Larmor frequency spectrometer. The HSQC experiments were recorded on a sample of two cyclopropane derivatives with 256 t_1 time increments for a spectral window of 150 ppm, an offset of 75 ppm and two scans per increment. The recovery delay was set to 3 s for a total acquisition time of 30 min. The DQF-COSY experiments were recorded for a sample of cyclosporine-A using 128 time increments over a spectral window of 10 ppm with two scans per increments. The recovery delay was set to 3 s for a total acquisition time of 17 min. The hard pulse duration were 15 and 10 μs for the ^{1}H and ^{13}C channels respectively. All pulse programs and spectra are available as Supplementary Material.

Supplementary Material

Beside the material mentioned in the article, the experimental spectra and the Matalb/Octave programs used for the preparation of the figures, a set of movies representing the dephasing of magnetization during pulses were included in the supplementary material and the Github repository https://github.com/Gr-Jeannerat-unige/SuppDataFOPAphase.

Acknowledgements

Kirill Sheberstov thanks Dmitry A. Cheshkov for private communications. We thank the SNSF (grant number 200020-126525, 206021-128746 and 200021-147069), the *Section de chimie* of the University of Geneva and the State of Geneva for funding. We thank Bruker Biospin (Fällanden, Switzerland) and the Department of physical chemistry for their contributions to the 300 MHz spectrometer of the group Jeannerat and Marion Pupier for corrections to the manuscript.

References

[1] T. D. W. Claridge, *High Resolution NMR Techniques in Organic Chemistry, Vol. 27*, Pergamon Press, Oxford, **2009**.
[2] J. Keeler, *Understanding NMR spectroscopy*, Wiley, Chichester, **2016**.
[3] M. H. Levitt, *Spin dynamics*, Wiley, Chichester, **2013**.
[4] R. R. Ernst, G. Bodenhausen, A. Wokaun, *Principles of Nuclear Magnetic Resonance in One and Two Dimensions*, Clarendon Press, Oxford, **1987**.
[5] D. Marion, K. Wüthrich, *Biochem. Biophys. Res. Comm.* **1983**, *113*, 967-974.
[6] G. Bodenhausen, R. L. Vold, R. R. Vold, *J. Magn. Reson.* **1980**, *37*, 93-106. doi: Doi 10.1016/0022-2364(80)90096-7
[7] P. Pfändler, G. Bodenhausen, *Magn. Reson. Chem.* **1988**, *26*, 888-894.
[8] G. Bodenhausen, *Prog. Nucl. Magn. Reson. Spectrosc.* **1980**, *14*, 137-173. doi: 10.1016/0079-6565(80)80007-0
[9] D. P. Weitekamp, *Adv. Magn. Reson.* **1983**, *11*, 111-274.
[10] M. H. Levitt, *J. Magn. Reson.* **1997**, *126*, 164-182. doi: 10.1006/jmre.1997.1161
[11] M. H. Levitt, O. G. Johannessen, *J. Magn. Reson.* **2000**, *142*, 190-194. doi: 10.1006/jmre.1999.1929
[12] R. R. Ernst, W. A. Anderson, *Rev. Sci. Instr.* **1966**, *37*, 93-102. doi: 10.1063/1.1719961
[13] D. Jeannerat, in *Encyclopedia of Magnetic Resonance, Vol. 6* (Ed.: G. A. Morris), John Wiley, Chichester, **2017**, pp. 161-172.

[14] T.-C. L. Wang, C. E. Cottrell, A. G. Marshall, *Comput. Chem.* **1983**, *7*, 183-197. doi: 10.1016/0097-8485(83)85011-6
[15] M. J. Thrippleton, J. Keeler, *Angew. Chem. Int. Ed. Engl.* **2003**, *42*, 3938-3941. doi: 10.1002/anie.200351947
[16] L. Emsley, G. Bodenhausen, *J. Magn. Reson.* **1989**, *82*, 211-221.
[17] S. Wimperis, G. Bodenhausen, *J. Magn. Reson.* **1987**, *71*, 355-359.
[18] H. Hu, A. J. Shaka, *J. Magn. Reson.* **1999**, *136*, 54-62.
[19] R. Tycko, H. M. Cho, E. Schneider, A. Pines, *J. Magn. Reson.* **1985**, *61*, 90-101. doi: 10.1016/0022-2364(85)90270-7
[20] M. H. Levitt, *eMagRes* **2007**. doi: 10.1002/9780470034590.emrstm0086
[21] M. H. Levitt, *Prog. NMR Spectrosc.* **1986**, *18*, 61-122.
[22] R. Freeman, *Chem. Rev.* **1991**, *91*, 1397-1412. doi: DOI 10.1021/cr00007a006
[23] L. Emsley, G. Bodenhausen, *J. Magn. Reson.* **1992**, *97*, 135-148.
[24] Z. Wang, J. S. Leigh, **1989**, *82*, 174-179. doi: 10.1016/0022-2364(89)90179-0
[25] V. L. Ermakov, J. M. Boehlen, G. Bodenhausen, *J. Magn. Reson., Ser. A* **1993**, *103*, 226-229.
[26] R. Fu, V. L. Ermakov, G. Bodenhausen, *Solid State Nucl. Magn. Reson.* **1996**, *7*, 1-10.
[27] D. Suter, G. C. Chingas, R. A. Harris, A. Pines, *Mol. Phys.* **1987**, *61*, 1327-1340. doi: 10.1080/00268978700101831
[28] C. J. Turner, H. D. W. Hill, *J. Magn. Reson.* **1986**, *66*, 410-421. doi: 10.1016/0022-2364(86)90185-X
[29] L. Gengying, X. Haibin, *Rev. Sci. Instrum.* **1999**, *70*, 1511-1513. doi: 10.1063/1.1149615
[30] A. G. Redfield, S. D. Kunz, *J. Magn. Reson.* **1975**, *19*, 250-254.
[31] M.-A. Delsuc, *J. Magn. Reson.* **1988**, *77*, 119-124. doi: 10.1016/0022-2364(88)90036-4
[32] D. J. States, R. A. Haberkorn, D. J. Ruben, *J. Magn. Reson.* **1982**, *48*, 286-292. doi: 10.1016/0022-2364(82)90279-7
[33] J. Keeler, D. Neuhaus, *J. Magn. Reson.* **1985**, *63*, 454-472. doi: Doi 10.1016/0022-2364(85)90236-7
[34] D. Jeannerat, in *Encyclopedia of Magnetic Resonance* (Ed.: G. A. Morris), John Wiley, Chichester, **2011**.
[35] R. E. Hurd, *J. Magn. Reson* **1990**, *87*, 422-428.
[36] M. v. Kienlin, C. T. W. Moonen, A. van der Toorn, P. C. M. van Zijl, *J. Magn. Reson.* **1991**, *93*, 423-429. doi: 10.1016/0008-6215(93)80114-T
[37] A. Bax, M. Ikura, L. E. Kay, G. Zhu, *J. Magn. Reson.* **1991**, *91*, 174-178. doi: 10.1016/0022-2364(91)90422-P
[38] E. Guardiola Sistare, PhD thesis, University of Geneva (Geneva), **2019**.
[39] M. Foroozandeh, D. Jeannerat, *Magn. Reson. Chem.* **2015**, *53*, 894-900. doi: 10.1002/mrc.4283

Graphical abstract

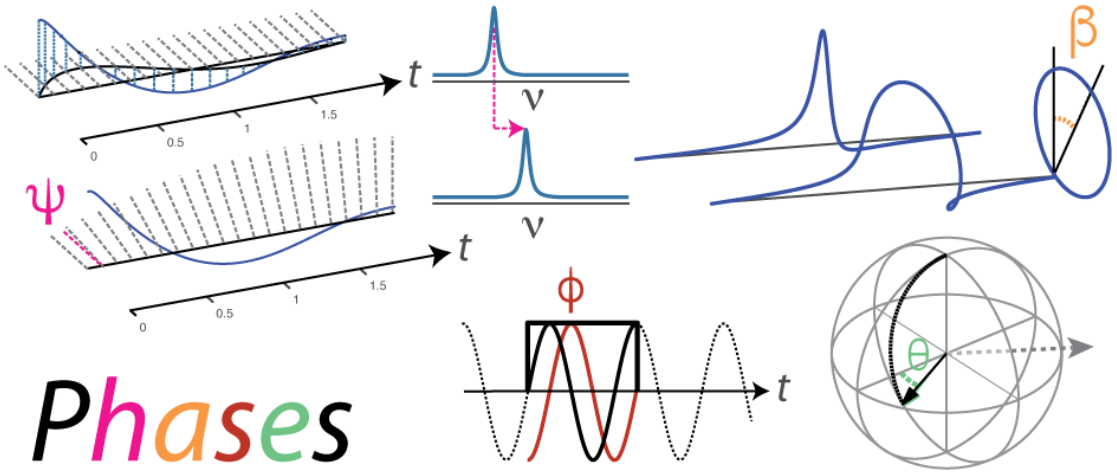

Supplementary Material

Everything you wanted to know about phase and reference frequency in one- and two-dimensional NMR Spectroscopy

Kirill F. Sheberstov [a], Eduard Guardiola Sistare [b], Damien Jeannerat [b,*]

[a] Johannes Gutenberg-Universität, Mainz, 55099, Germany

[b] Department of Organic Chemistry, University of Geneva, Geneva, 1211, Switzerland.

Table of content

1 Phase modulation of pulses

Besides the time-constant shift of the radiofrequency that determines the phase of a pulse, a time-dependent phase shift can change its effective frequency. Phase shifters are used to produce a phase modulation resulting in a shift of the pulse frequency. Instead of the original value given by the synthesizer frequency ν_{cf} the effective frequency can be adjusted to ν_p. It is obtained by applying a linear time dependency on the phases:

$$\cos\left(2\pi\,\nu_{cf}t + \varphi(t)\right) = \cos\left(2\pi\,\nu_{cf}t + 2\pi\,\delta t\right) = \cos\left(2\pi\,\nu_p t\right)$$

2 Phase shift of the magnetization as a function of the offset

The deviation from linearity of the phase shift is no more than 3° over $0.5\,\nu_{rf}$ (See Figure S1). This is small enough to make a first-order correction with a value of -57 quite satisfactory for the most common isotopes ^{1}H, ^{13}C. Indeed, $0.5\,\nu_{rf}$ = 12'500 Hz and corresponds to +/– 5 ppm at 500 MHz proton Larmor frequency and +/– 100 ppm at 125 MHz carbon Larmor frequency. A phase correction over a much broader range would require a correction based on the full phase shift function shown in Figure S1.

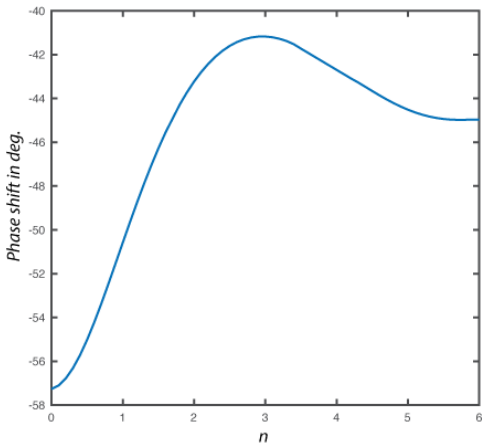

Figure S1. Phase shift of signals as a function of the offset given as $n = \Delta/\nu_{rf}$.

3 Evolution and profiles of 270° pulses

The bandwidth of a 270° pulse is much smaller than of a 90° pulse (see Figure S2). The 90% excitation covers ± 0.38, instead of $\pm 1.58\,\nu_{rf}$, but for the y component alone, the difference is much smaller ± 0.38 instead of $\pm 0.5\,\nu_{rf}$. In other words, the bandwidth corresponding to a "good" excitation (*i.e.* with signal having the same x phase) is larger. Indeed, the Mx and the absolute-value profiles are almost indistinguishable, unlike for 90° pulses. This property of self-refocusing is particularly useful when using selective pulses, that is for pulses with much longer evolution.

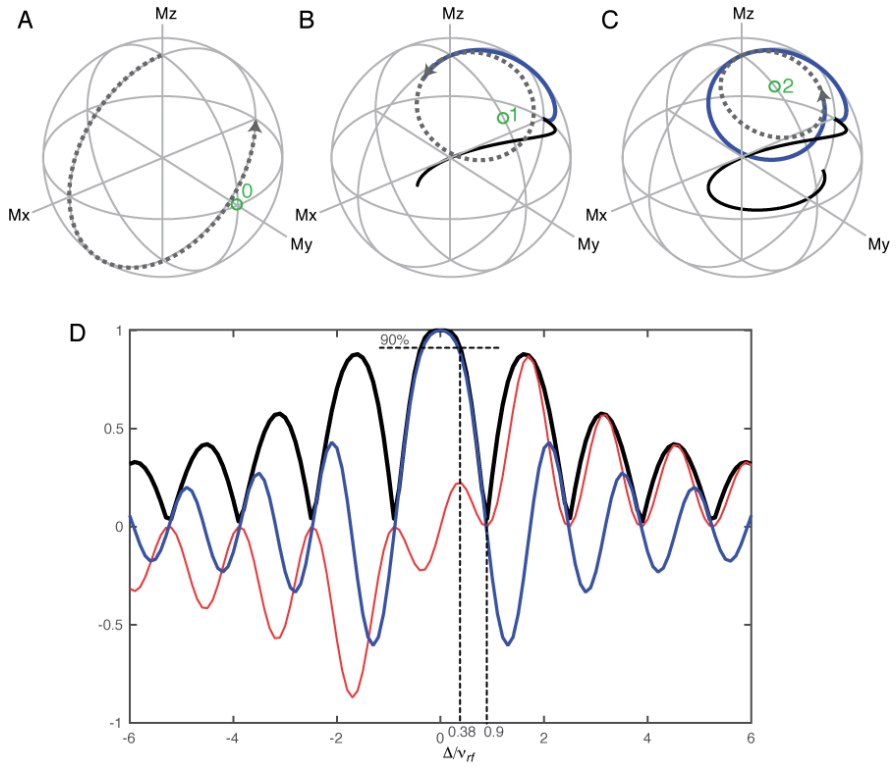

Figure S2 (A-C) Bloch spheres and (D) excitation profiles of the final position of the magnetization following a 270° pulse as a function of ν_{rf}. The full trajectory of the magnetizations (dotted lines in A-C) were plotted for integer values of ν_{rf} equal to 0 (A), 1 (B) and 2 (C). Open green circles indicate the direction of the effective-field vectors about which the magnetization (dotted lines) precesses. The blue lines and their black projections on the *x/y* plane in B and C correspond to the end point of the magnetization for ν_{rf} values ranging from 0 to 1 (in B) and 0 to 2 (in C). In (D), the broad line corresponds to the norm of the vector formed of the M_x (blue) and M_y (red) components of the magnetization. Note that the *x*-component is quite small within the central bell and that the boundaries of the 90% excitation are located at $\pm 0.38 \cdot \nu_{rf}$ while the zero is found at $\pm 0.9 \cdot \nu_{rf}$.

4 Direct quadrature detection

Let us consider a simple case of just one signal in the spectrum produced by a spin-1/2 with the Larmor frequency ν_0. The phase of the pulse is set to $\varphi_p = \frac{\pi}{2}$, corresponding to y axis in a rotating frame with a frequency ν_{cf}. This situation is illustrated in Figure 2 of the main text. We consider the action of a hard 90 degree pulse

$$B_1(t) = -\frac{1}{4\gamma\tau_p}\sin\left(2\pi\,\nu_{cf}\,t\right)$$

and neglect the off-resonance effects, so the magnetization is flipped to the x axis in the rotating frame. The probe coil picks up the evolution of the signal, resulting in a signal:

$$s(t) \propto \cos(2\pi\, \nu_0 t) \exp\,(-t/T_2)$$

where T_2 is the transverse relaxation time. It is impossible to determine the sense of the precession using a single coil, but in NMR we usually do not worry about the absolute direction of Larmor precession. Instead, quadrature detector subtracts the carrier frequency, as described below.

The Figure S3 illustrates what happens to the signal. Apart from the signal $S(t)$ itself, there is a reference signal, produced by the synthesizer. We consider the case when the receiver has a phase $\varphi_{rec} = 0$, so it is as if the detector was along the x axis of the rotating frame. In the laboratory frame, the reference signal is thus given by:

$$ref1(t) \propto \cos\big(2\pi\, \nu_{cf} t\big).$$

Both $s(t)$ and $ref(t)$ are then duplicated, and one of the components of the reference signal is additionally shifted by $\frac{\pi}{2}$ to produce:

$$ref2(t) \propto -\sin\big(2\pi\, \nu_{cf} t\big).$$

The mixers perform a mutual amplitude modulation of the $S(t)$ and $ref(t)$ signals, thus producing the "real" and "imaginary" parts of the complex FID:

$$Re(t) \propto \cos\big(2\pi\, \nu_{cf} t\big) \cos(2\pi\, \nu_0 t) \exp\,(-t/T_2)$$

$$Im(t) \propto -\sin\big(2\pi\, \nu_{cf} t\big) \cos(2\pi\, \nu_0 t) \exp\,(-t/T_2).$$

A low-pass filter removes high-frequency oscillations and trigonometric properties allow to write

$$Re(t) = \cos\big(2\pi\, \{\nu_0 - \nu_{cf}\} t\big) \exp\,(-t/T_2)$$

$$Im(t) = \sin\big(2\pi\, \{\nu_0 - \nu_{cf}\} t\big) \exp\,(-t/T_2).$$

The reader may verify how these functions depend on the relative values of ν_{cf} and ν_0. The Figure 5 of the main text illustrates these different cases. Thus, quadrature detection conserves the information about the sign of the frequency difference with the carrier frequency.

In modern spectrometers this scheme is a bit more complex, consisting of two steps to subtract the frequency: In the first step an intermediate frequency, which is far from spectral range, is subtracted in order to avoid the problems with frequency discrimination. The signal is then converted by an analog-to-digital converter (ADC) and further frequency subtraction is performed digitally. Digital quadrature detection generates much cleaner spectra.[1]

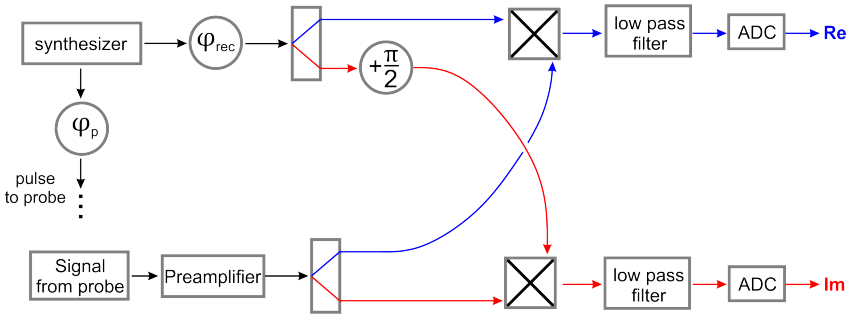

Figure S3. Electronic scheme of simple quadrature detection.

5 Influence of the phase of the detector on the phase of detected signals

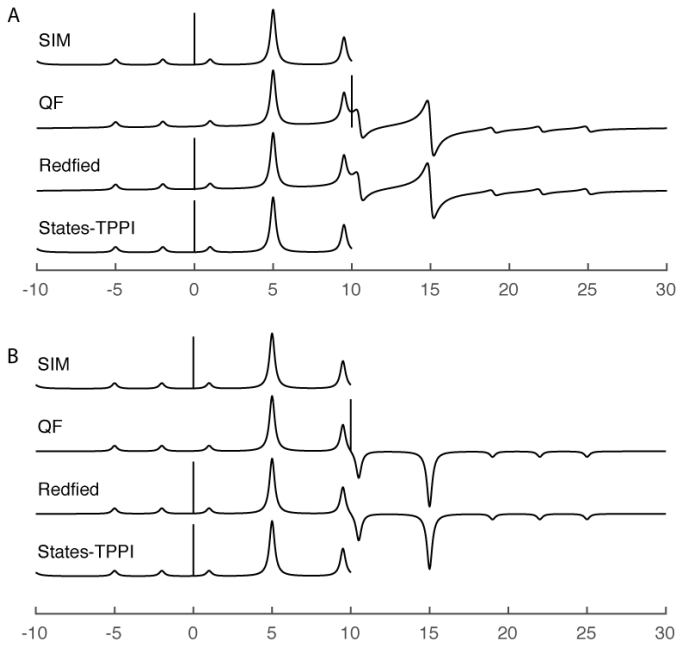

Figure S4 Spectra obtained after Fourier transformation of the FID acquired using a detector phase set to 45 (A) and 90° (B) relative to the excitation pulse. (See Figure 6 of the main text for more details).

6 Demonstration of the apparent frequency shift obtained by phase incrementation

At the detected times

$$t_n = n \cdot dw,$$

where n is an integer ranging from [0 : 2N–1], and N the number of detected points, the signal with a Δ_0 frequency is

$$S_n \propto cos(2\pi \Delta_0 \cdot n \cdot dw)$$

The Redfield trick multiplies the detected points with a coefficient

$$cos\left(2\pi\, \nu_{cf} \cdot n \cdot dw + \, n \cdot \psi\right)$$

which, is evaluated after the filtering of high-frequency components to a detected signal

$$S_n \propto cos\left(2\pi(\, \Delta_0 - \nu_{cf} - \frac{\psi}{2\pi}\frac{1}{dw}) \cdot n \cdot dw\right).$$

The frequency shift caused by the phase incrementation is therefore given by the following term:

$$\upsilon_{Red}(\psi) = \frac{\psi}{2\pi}\frac{1}{dw}.$$

After combination with the Nyquist condition, it becomes:

$$\upsilon_{Red}(\psi) = \frac{2SW\psi}{2\pi}.$$

This completes the demonstration that a phase incrementation of $\pi/2$ shifts the reference frequency from the center to the side of the spectrum because

$$\upsilon_{Red}(\pi/2) = sw/2.$$

7 Frequency dependence of the F1-phase of peaks when the initial t_1 increment is non-zero

Compared to a normal spectrum (top left of Figure S5), spectra recorded with $t_1^{initial} > 0$ show peaks with F1 phases proportional to the difference between their frequency and the carrier frequency (black line). This phase is represented in Figure S5 by the angle φ between the cross-sections running from the blue to the red sides of the spectra and the horizontal plane (left spectra in Figure S5).

One can consider aliased spectra (right parts of Figure S5) as spectra that are rolled on a cylinder and cut at the opposite side of the carrier frequency.[2] When $t_1^{initial} = 0$, all peaks are positive with a pure-absorption lineshape as shows the flat surface of the cylinder in the top-right part of Figure S5.

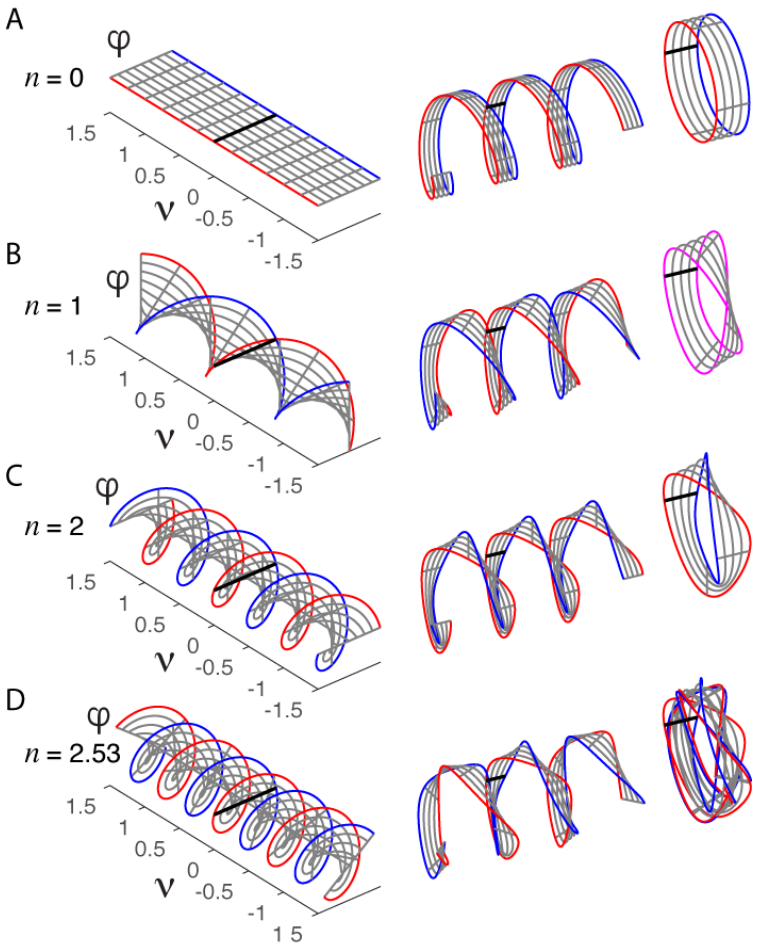

Figure S5 (left) Representation of the F1-phase of signals of 2D spectra. (A) The cross-section is horizontal when the phase is zero. In other cases, the phase is represented by the angle between the horizon and the cross-section running from the blue to the red sides. The phase varies linearly across the F1 boundaries, by $n \cdot f \cdot 180°$ where $f = 3$ and n increases from top to bottom. When reducing the spectral width by a factor f, the spectra (left) look as if they were rolled on a rod with a perimeter equal to the aliased spectral width (middle) and aligned to represent the aliased spectra (right). When the red and blue sides superpose (Möbius strip) they were plotted in magenta (right part in B).

When $t_1^{init.} = \frac{1}{2} dw$, the phase of signals in the aliased spectrum changes by 180° across the aliased spectrum (second row of Figure S5, $n = 1$). Because walking over a Möbius strip changes of side at every turn, signals with odd and even aliasing order n will have opposite signs (their phases increase by 180° at each turn) as indicated in Table 1 of the main text. A 180° first-order phase correction can be applied and results in pure absorption for all signals. An advantage of this choice is that the change of sign can be used to identify aliased peak. This is commonly done in protein NMR spectroscopy where HSQC spectra are often recorded with two-fold aliasing in the ^{15}N dimension.

When $t_1^{init.} = dw$, (third row, $n = 2$) the phases of signals in the aliased spectrum changes by 360° across the aliased spectrum (third row). Because of the double changes of side of the strip at every cycle (right) all signals have the same sign

after phase correction. This may be a better choice when signal cancellation is of concern.

When $t_1^{init.}$ is set to an arbitrary value (last row in Figure S5) the phases of signals in the aliased spectrum is different at each turn. The spectrum is therefore impossible to phase in the indirect F1 dimension. Note that these F1-phases carry information on the aliasing order[2], *i.e.* the region of the spectrum where the signal comes from. Combined with the F1 position of signals in the aliased spectrum, it has been used to reconstruct full high-resolution spectra from aliased spectra.[3]

8 FOPA of DQF-COSY experiments

The frequency offset by phase adjustment (FOPA) was applied to HSQC (Figure 10 of the main article) and DQF-COSY experiments (Figures S6 and S7).

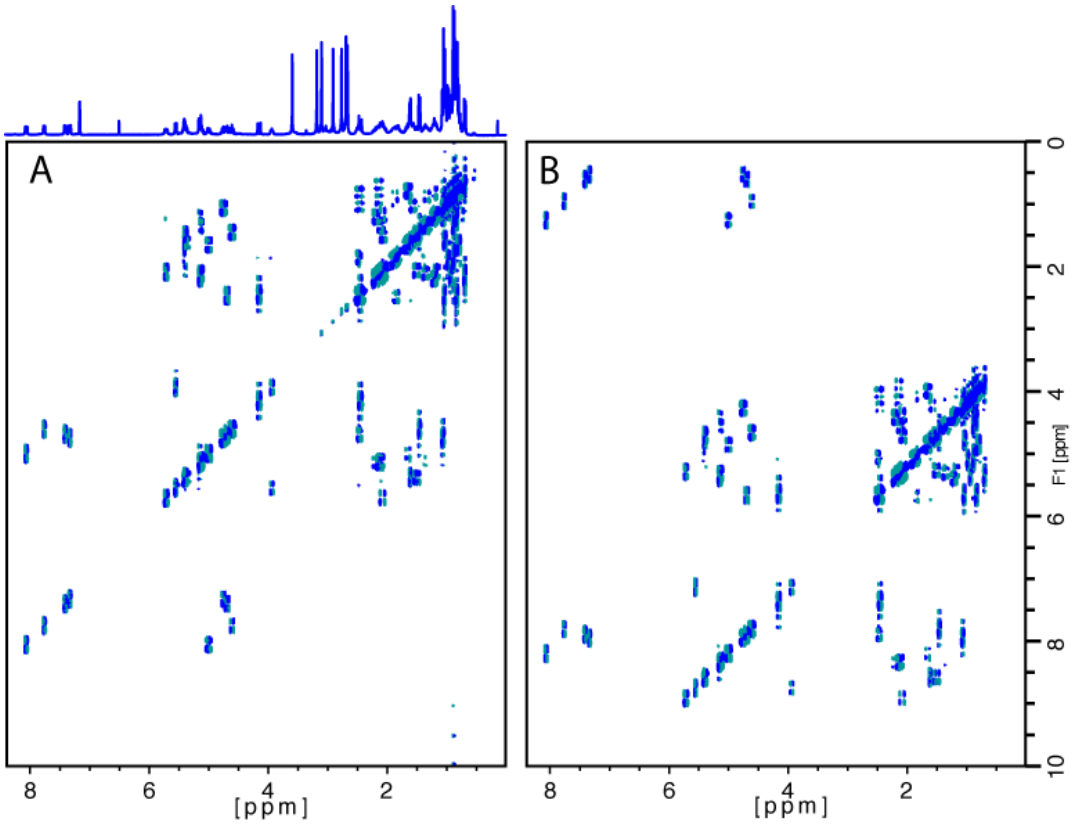

Figure S6 DQF COSY spectra recorded without (A) and with (B) a shift of the apparent carrier frequency obtained by adjustment of the phase of pulses. The center of the spectrum was moved to 1.8 ppm in B. The quadrature was obtained using the Echo/Anti-echo method.

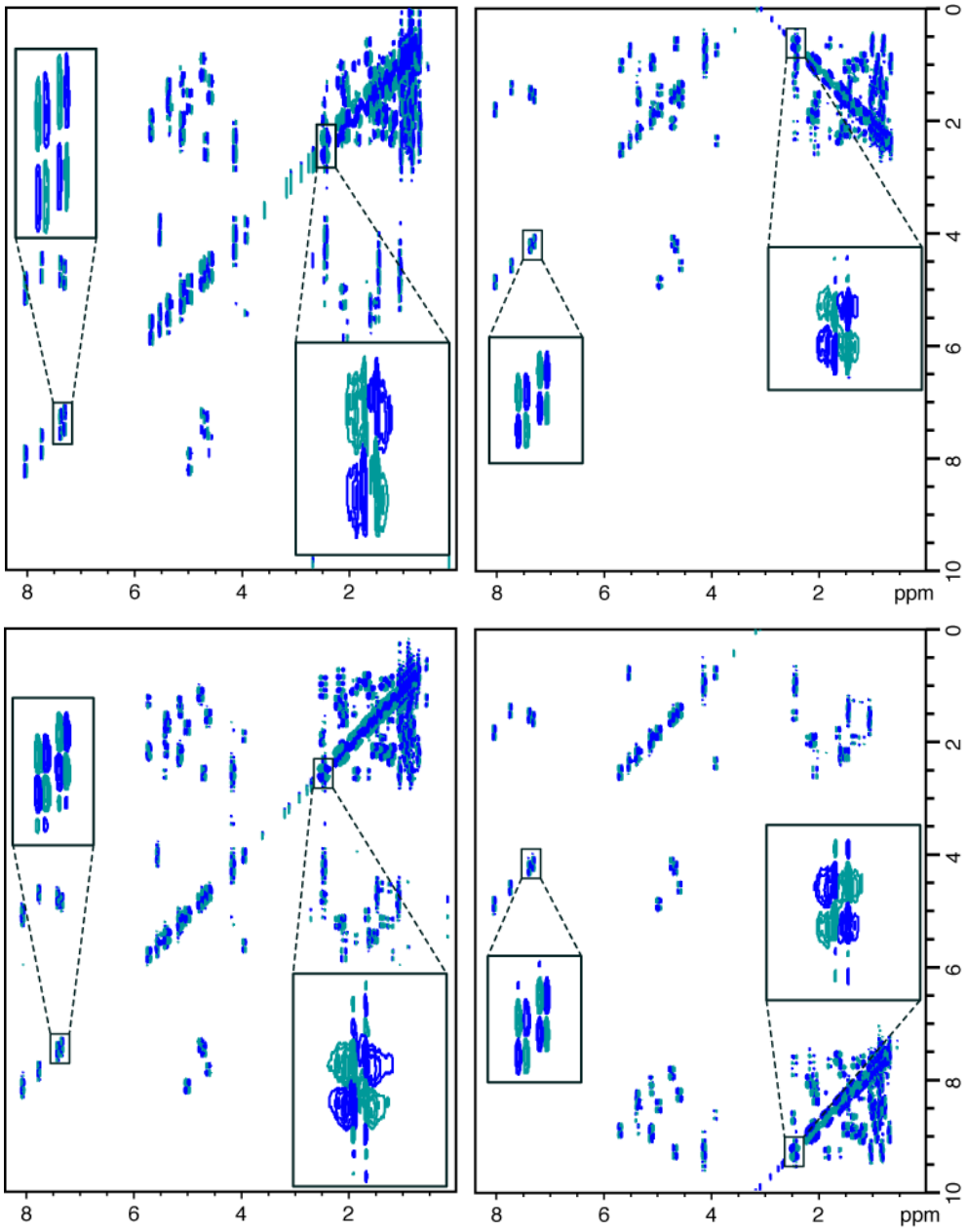
8
6
4
2
ppm
0
2
4
6
8
10

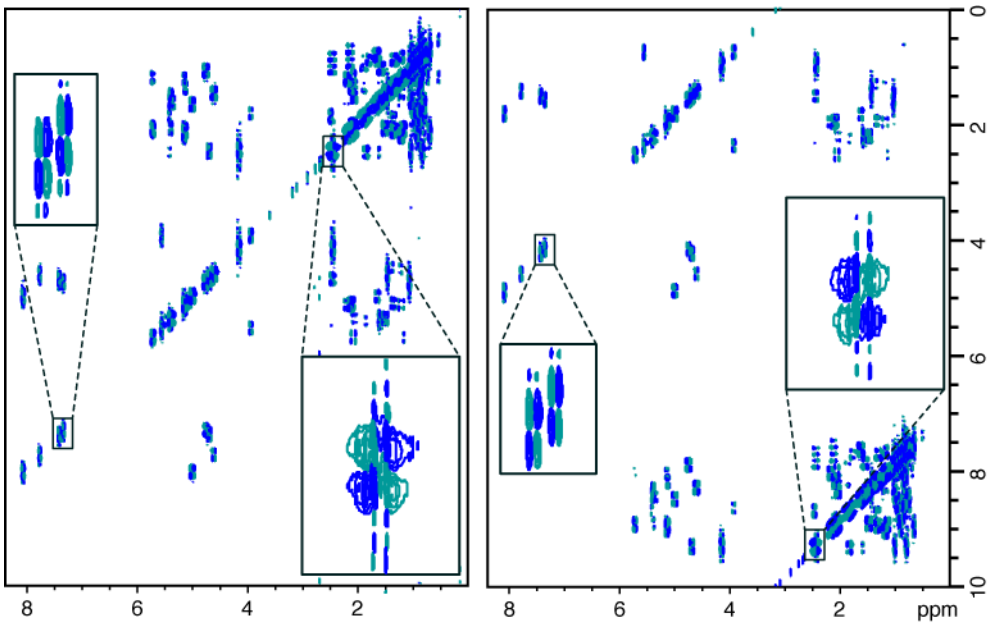

Figure S7 DQF COSY spectra recorded without (left) and with (right) a shift of the apparent carrier frequency obtained by adjustment of the phase of pulses. The center of the spectrum was moved to 8.15 ppm in the right spectra. The quadrature was obtained using (from top to bottom) the TPPI, States and States-TPPI method respectively. Note the folding (instead of aliasing) with the TPPI quadrature, and the inversion of the signs of aliased signals with the States and States-TPPI quadratures.

The pulse programs and spectra (including DQF-COSY spectra recorded with the States, the TPPI and the States-TPPI methods) are available on GitHub: https://github.com/Gr-Jeannerat-unige/SuppDataFOPAphase.

9 Pulse sequences including FOPA

Phase adjustment compatible with Topspin version 2.1pl8 are explained and provided in the following section for HSQC E/AE and DQF-COSY E/AE, States-TPPI, States and TPPI experiments. It is using the first pulse after the end of the t_1 evolution time delay as reference.

The phase adjustment takes the time between the shifted and the reference pulse, the desired reference frequency (`cnst21`) and the center of the spectrum (`cnst22=o1/bf1`) into account.

The difference in frequency is calculated as

`"cnstXX=(cnst22-cnst21)*bf1"`

when pulses follow the reference pulse and as

`"cnstXX=(-cnst22+cnst21)*bf1"`

otherwise.

The phase shift is calculated as

`"cnstYY = 360* cnstXX*((`*Sum of delays in s*`) + 0.000001* (`*sum of pulses in us*`))"`

Example:

```
"cnst22=o1/bf1"
"cnst23=(cnst22-cnst21)*bf1"
"cnst24=(-cnst22+cnst21)*bf1"
"DELTA=p16+d16+d13"
"cnst29=360*cnst24*(d0+0.000001*(p1/2+p1/2))"
"cnst30=360*cnst23*(d13+d16+0.000001*(p1/2+p16+p2/2))"
4uip6+cnst29
p1ph1+ph6
d0
p1 ph2 ;REFERENCE PULSE PHASE
DELTA*0.5 UNBLKGRAD
DELTA*0.5 ip4+cnst30
p2 ph4
```

When a phase `phX` is modified by the quadrature loop, one should use a dummy phase `phY` which is taking the FOPA into account

```
4u iphY + cnstYY
```

and then add it to ***phX*** when the pulse is used with

```
p1 phX + phY
```

When the receiver phase has to be incremented, it cannot be done by directly modifying `ph31` because it is only allowing values equal to 0, 90, 180 and 270 degrees. But one can use `ph30` for the FOPA and use the following command for detection:

go = 2 ph31 `ph30:r`

10 POPA pulse sequences

hsqc_ea_FOPA_2_0.esg

```
;$CLASS=HighRes
;$DIM=2D
;$TYPE=
;$SUBTYPE=
;$COMMENT=
#include <Avance.incl>
#include <Grad.incl>
#include <Delay.incl>
"p2=p1*2"
"p4=p3*2"
"d4=1s/(cnst2*4)"
"d0=3u"
"d10=3u"
"d11=30m"
"d12=3u"
"d13=4u"
"in0=(inf1/2)"
"in10=in0/cnst9"
"cnst22=o2/bf2"
"cnst23=(cnst22-cnst21)*sfo2" ;for ref. to calc.
"cnst24=(-cnst22+cnst21)*sfo2" ;for calc. to ref.
"DELTA1=d4-p16-larger(p2,p14)/2-8u"
"DELTA2=d4-larger(p2,p14)/2"
"DELTA3=d4-30u-larger(p2,p14)/2"
"DELTA=p16+d16"
1 ze
  d11 pl12:f2
2 d1 do:f2
3
  "cnst30  =  360*(cnst24)*(2*d0  +  d13  +  d16  +
0.000001*(p3/2 + p2 + p16 + p24/2))"
  "cnst31  =  360*(cnst23)*(d13  +  2*d12  +  d16  +
0.000001*(p24/2 + p16 + p2 + p3/2))"
    (p1 ph1)
    DELTA2 pl0:f2
    4u
    (center (p2 ph1) (p14:sp3 ph6):f2 )
    4u
    DELTA2*0.5 pl2:f2 UNBLKGRAD
    DELTA2*0.5 ip9+cnst30
  ; p28 ph1
  ; 4u
    (p1 ph2)
    (p3 ph3+ph9):f2 ;ph9
  ; first evolution time - t1
    d0
    (p2 ph5)
    d0
```

```
      p16:gp1*EA
      d16 pl0:f2
      4u
      (p24:sp7 ph7):f2 ;REFERENCE PHASE
      4u
      DELTA*0.5 pl2:f2
      DELTA*0.5 ip9+cnst31
      3u
      (p2 ph5)
      3u
      (p3 ph9):f2
      (p1 ph1)
      DELTA2 pl0:f2
      (center (p2 ph1) (p14:sp3 ph8):f2 )
      4u
      p16:gp2
      DELTA1 pl12:f2
      4u BLKGRAD
      go=2 ph31 cpd2:f2
      d1 do:f2 mc #0 to 2
         F1EA(igrad EA, id0 & ip3*2 & ip6*2 & ip31*2)
   exit

   ph1=0
   ph2=1
   ph3=0 2
   ph4=0 0 0 0 2 2 2 2
   ph5=0 0 2 2
   ph6=0
   ph7=0 0 0 0 2 2 2 2
   ph8=0
   ph9=0 ;incrementation dummy phase for ph3
   ph31=0 2 0 2 2 0 2 0
   ;pl0 : 120dB
   ;pl1 : f1 channel - power level for pulse (default)
   ;pl2 : f2 channel - power level for pulse (default)
   ;pl3 : f3 channel - power level for pulse (default)
   ;pl12: f2 channel - power level for CPD/BB decoupling
   ;sp3:  f2  channel  -  shaped  pulse  180  degree  for
inversion
   ;sp7:  f2  channel  -  shaped  pulse  180  degree  for
refocussing
   ;p1 : f1 channel -  90 degree high power pulse
   ;p2 : f1 channel - 180 degree high power pulse
   ;p3 : f2 channel -  90 degree high power pulse
   ;p14:  f2  channel  -  180  degree  shaped  pulse  for
inversion
   ;p16: homospoil/gradient pulse
   ;p22: f3 channel - 180 degree high power pulse
   ;p24:  f2  channel  -  180  degree  shaped  pulse  for
refocussing
   ;p28: f1 channel - trim pulse
```

```
   ;d0 : incremented delay (2D)                [3 usec]
   ;d1 : relaxation delay; 1-5 * T1
   ;d4 : 1/(4J)XH
   ;d11: delay for disk I/O                    [30 msec]
   ;d16: delay for homospoil/gradient recovery
   ;cnst2: = J(XH)
   ;cnst21: F1 reference chemical shift
   ;inf1: 1/SW(X) = 2 * DW(X)
   ;in0: 1/(2 * SW(X)) = DW(X)
   ;nd0: 2
   ;NS: 1 * n
   ;DS: >= 16
   ;td1: number of experiments
   ;FnMODE: echo-antiecho
   ;cpd2: decoupling according to sequence defined by
cpdprg2
   ;pcpd2: f2 channel - 90 degree pulse for decoupling
sequence
   ;use gradient ratio:  gp 1 : gp 2
   ;             80 : 20.1    for C-13
   ;             80 :  8.1    for N-15
   ;for z-only gradients:
   ;gpz1: 80%
   ;gpz2: 20.1% for C-13, 8.1% for N-15
   ;use gradient files:
   ;gpnam1: SINE.100
   ;gpnam2: SINE.100
```

DQF-COSY_ea_FOPA_2_0.esg

```
;$CLASS=HighRes
;$DIM=2D
;$TYPE=
;$SUBTYPE=
;$COMMENT=

#include <Avance.incl>
#include <Grad.incl>
#include <Delay.incl>

"p2=p1*2"
"d11=30m"
"d12=3u" ;inicial d0
"d13=4u"
"in0=inf1"
"d0=3u"
"cnst22=o1/bf1"
"cnst23=(cnst22-cnst21)*bf1" ;ref. to calc.
"cnst24=(-cnst22+cnst21)*bf1" ;calc. to ref.
"DELTA=p16+d16+d0"
"DELTA1=p16+d16+8u"

1 ze
2 d11
3
"cnst29   =   360*cnst24*(d12   +   d0   +   2*d16   +
0.000001*(p1/2 + p16 + p2 + p16 + p1/2))"
"cnst30 = 360*cnst24*(d0 + d16 + 0.000001*(p2/2 + p16
+ p1/2))"
"cnst31 = 360*cnst23*(2*d13 + d16 + 0.000001*(p1/2 +
p16 + p2/2))"
"cnst32 = 360*cnst23*(4*d13 + 2*d16 + 0.000001*(p1/2 +
p16 + p2 + p16 + p1/2))"
"cnst33 = 360*cnst23*(6*d13 + 3*d16 + 0.000001*(p1/2 +
p16 + p2 + p16 + p1 + p16 + p2/2))"
"cnst34 = 360*cnst23*(8*d13 + 4*d16 + 0.000001*(p1/2 +
p16 + p2 + p16 + p1 + p16 + p2 + p16))"

4u ip3+cnst29
  d1
  50u UNBLKGRAD
  p1 ph1+ph3
  DELTA   ip3+cnst30
  p2 ph2+ph3
  d0
  p16:gp1*EA
  d16
  p1 ph2 ;REFERENCE PULSE PHASE
  DELTA1   ip3+cnst31
  p2 ph2+ph3
  8u
```

```
  p16:gp2
  d16   ip3+cnst32
  p1 ph2+ph3
  DELTA1   ip3+cnst33
  p2 ph2+ph3
  4u
  p16:gp3
  d16   ip30+cnst34
  4u BLKGRAD
  go=2 ph31 ph30:r
  d11 mc #0 to 2 F1EA(igrad EA, id0 & ip1*2 & ip31*2)
exit

ph1=0 2
ph2=0
ph3=0 ;incrementation dummy phase for ph1 and ph2
ph30=0 ;incrementation phase for ph31
ph31=0 2

;pl1 : f1 channel - power level for pulse (default)
;p1 : f1 channel -  90 degree high power pulse
;p2 : f1 channel - 180 degree high power pulse
;p16: homospoil/gradient pulse
;d0 : incremented delay (2D)              [3 usec]
;d1 : relaxation delay; 1-5 * T1
;d11: delay for disk I/O                  [30 msec]
;d13: short delay                         [4 usec]
;d16: delay for homospoil/gradient recovery
;cnst21: F1 reference chemical shift
;inf1: 1/SW = 2 * DW
;in0: 1/(1 * SW) = 2 * DW
;nd0: 1
;NS: 8 * n
;DS: 16
;td1: number of experiments
;FnMODE: echo-antiecho

;use gradient ratio:  gp 1 : gp 2 : gp 3
;                30 :   10 :   50

;for z-only gradients:
;gpz1: 30%
;gpz2: 10%
;gpz3: 50%

;use gradient files:
;gpnam1: SINE.100
;gpnam2: SINE.100
;gpnam3: SINE.100
```

DQF-COSY_ph_FOPA_2_0.esg

```
;$CLASS=HighRes
;$DIM=2D
;$TYPE=
;$SUBTYPE=
;$COMMENT=

#include <Avance.incl>
#include <Delay.incl>
#include <Grad.incl>

"p2=p1*2"
"d13=4u"
"in0=inf1"
"d0=in0/2-p1*4/3.1416"
"cnst22=o1/bf1"
"cnst23=(cnst22-cnst21)*bf1" ;ref. to calc.
"cnst24=(-cnst22+cnst21)*bf1" ;calc. to ref.
"DELTA=p16+d16+d13"

1 ze
2 d1
3
"cnst29 = 360*cnst24*(d0 + 0.000001*(p1/2 + p1/2))"
"cnst30 = 360*cnst23*(d13 + d16 + 0.000001*(p1/2 + p16
+ p2/2))"
"cnst31 = 360*cnst23*(2*d13 + 2*d16 + 0.000001*(p1/2 +
p16 + p2 + p16 + p1/2))"
"cnst32 = 360*cnst23*(3*d13 + 3*d16 + 0.000001*(p1/2 +
p16 + p2 + p16 + p1 + p16 + p2/2))"
"cnst33 = 360*cnst23*(4*d13 + 4*d16 + 0.000001*(p1/2 +
p16 + p2 + p16 + p1 + p16 + p2 + p16))"

  4u ip6+cnst29
  p1 ph1+ph6
  d0
  p1 ph2 ;REFERENCE PULSE PHASE
  DELTA*0.5 UNBLKGRAD
  DELTA*0.5 ip4+cnst30
  p2 ph4
  d13
  p16:gp1
  d16 ip3+cnst31
  p1 ph3
  DELTA ip5+cnst32
  p2 ph5
  d13
  p16:gp2
  d16 ip30+cnst33
```

```
  4u BLKGRAD
  go=2 ph31 ph30:r
  d1 mc #0 to 2 F1PH(ip1, id0)
exit

ph1=1 3
ph2=0
ph3=1
ph4=0
ph5=0
ph6=0 ;incrementation dummy phase for ph1
ph30=0 ;incrementation phase for ph31
ph31=0 2

;pl1 : f1 channel - power level for pulse (default)
;p1 : f1 channel -  90 degree high power pulse
;p2 : f1 channel - 180 degree high power pulse
;p16: homospoil/gradient pulse
;d0 : incremented delay (2D)
;d1 : relaxation delay; 1-5 * T1
;d13: short delay                                  [4 usec]
;d16: delay for homospoil/gradient recovery
;cnst21: F1 reference chemical shift
;inf1: 1/SW = 2 * DW
;in0: 1/(1 * SW) = 2 * DW
;nd0: 1
;NS: 1 * n
;DS: 16
;td1: number of experiments
;FnMODE: States-TPPI, TPPI, States or QSEQ

;use gradient ratio:  gp 1 : gp 2
;             10 :   20   for double quantum filter
;             10 :   30   for triple quantum filter

;for z-only gradients:
;gpz1: 10%
;gpz2: 20% for DQF, 30% for TQF

;use gradient files:
;gpnam1: SINE.100
;gpnam2: SINE.100

;Processing

;PHC0(F1): 90
;PHC1(F1): -180
;FCOR(F1): 1
```

11 References

[1] L. Gengying, X. Haibin, *Rev. Sci. Instrum.* **1999**, *70*, 1511-1513. doi: 10.1063/1.1149615

[2] D. Jeannerat, in *Encyclopedia of Magnetic Resonance* (Ed.: G. A. Morris), John Wiley, Chichester, **2011**.

[3] K. Ramirez-Gualito, D. Jeannerat, *Magn. Reson. Chem.* **2015**, *51*, 901-907. doi: 10.1002/mrc.4301